Lead, zinc, and copper redistributions in soils along a deposition gradient from emissions of a Pb-Ag smelter decommissioned 100 years ago

Romain Gelly, Zuzana Fekiacova, Abel Guihou, Emmanuel Doelsch, Pierre Deschamps, Catherine Keller

Lead, zinc and copper redistributions in soils along a deposition gradient from emissions of a Pb-Ag smelter decommissioned 100 years ago

R. Gelly [a]***, *Z. Fekiacova* [1], *A. Guihou* [1], *E. Doelsch* [2], *P. Deschamps* [1], *C. Keller* [1]

(1) Aix Marseille Univ, CNRS, IRD, INRA, Coll France, CEREGE, BP 80, 13545 Aix-en-Provence cedex 04, France

(2) CIRAD, UPR Recyclage et risque, F-34398 Montpellier, France Recyclage et Risque, Univ Montpellier, CIRAD, Montpellier, France

Abstract

Sourcing and understanding the fate of anthropogenic metals in a historical contamination context is challenging. Here we combined elemental and isotopic (Pb, Zn, Cu) analyses with X-ray absorption spectroscopy (XAS) measurements (Zn) to trace the fate, in undisturbed soil profiles, of historical metal contamination emitted by a 167-year-old Pb-Ag smelter decommissioned 100 years ago located in the Calanques National Park (Marseilles, France). Lead isotopic measurements show that entire soil profiles were affected by 74 years of Pb emissions up to ~7 km from the smelter under the main NNW wind, and indicate particulate transfer down to 0.8 m at depth. This vertical mobility of anthropogenic Pb contrasts with previous studies where Pb was immobilized in surface horizons. The contribution of anthropogenic Pb to the total Pb concentration in soils was estimated at 95% in surface horizons, and 78% in the deepest horizons. Zinc isotopic signatures of past emissions, that are enriched in light isotopes compared to the natural geological background (-0.69 ±0.03‰ and -0.15 ±0.02‰, respectively), were detected only in the surface horizons of the studied soils. Using XAS analyses, we showed that anthropogenic Zn was transformed and immobilized in surface horizons as Zn-Layered Double Hydroxide, thus favoring the enrichment in heavy isotopes in these surface horizons. No clear evidence of copper contamination by the smelter was found and Cu isotopes point to a bedrock origin and a natural distribution of Cu concentrations.

Highlights:

- δPb, Zn, Cu in soils impacted by emissions 100 y ago from a smelter
- Pb contamination was detected 7 km away from the smelter and down the soil profiles

- Light δ^{66}Zn values were measured in the chimney and in soil surface horizons
- Precipitation of Zn-Layered Double Hydroxide prevented downwards migration of anthropogenic Zn
- Cu isotopes indicate its geogenic origin and redistribution in soils by pedogenesis

Keywords:
metal contamination, soil, stable isotopes, historical contamination, metal cycling, smelting

Introduction

Lead (Pb), zinc (Zn) and copper (Cu) are trace elements naturally present in soils at concentrations usually below 1000 mg kg^{-1} (Kabata-Pendias, 2011). They are also released by human activities through emission to the atmosphere or direct application (e.g. by smelting, fossil energy consumption and soil fertilization). Lead is toxic to living organisms even at low doses (World Health Organization et al., 1996). Zinc and Cu are micro-nutrients required in biochemical reactions, but their excessive concentrations lead to toxicity (World Health Organization et al., 1996). In soils, distinguishing between the natural and anthropogenic origins of Pb, Zn and Cu is still a challenge as pedogenetic processes redistribute metals within soil profiles and alter their speciation (Legros, 2007; Semlali et al., 2001). Yet, the distinction is essential for tracing the source of contamination and transfer in soils, and for identifying the potential risks of increased anthropogenic metal transfer in the environment and associated remediation plans.

Since the 1990s, Pb isotopes have proved to be powerful tracers of Pb contamination related to gasoline emissions (Erel et al., 1997; Luck and Ben Othman, 2002a; von Storch et al., 2003) and to emissions from industrial areas (Cloquet et al., 2006; Jeon et al., 2017; Wen et al., 2015).

Furthermore, Pb isotopes have been used for tracing the transport and redistribution of Pb in the atmosphere (Desenfant et al., 2006; Hamelin et al., 1997; Shotyk et al., 2002; Véron et al., 1999; Weiss et al., 2002). More recently, Cu and Zn isotopes were used to link increased metal concentrations in soils or sediments to the emissions of metallurgic plants (Araújo et al., 2018; Bigalke et al., 2010a; Juillot et al., 2011; Kříbek et al., 2018; Mihaljevič et al., 2018; Sivry et al., 2008; Sonke et al., 2008; Thapalia et al., 2010), or for sourcing metal particles from mining and tailing sites (Borrok et al., 2009; Kimball et al., 2009; Song et al., 2016; Viers et al., 2018). Anthropogenic Cu and Zn isotope tracing relies on large isotopic fractionation (Mattielli et al., 2009; Ochoa Gonzalez and Weiss, 2015; Shiel et al., 2010; Wiederhold, 2015) created during high-temperature industrial processes (e.g., smelting) generating particles emitted to the atmosphere, that are enriched in light isotopes and distinct from the isotopic signatures of soil and from any potential small isotopic fraction induced by natural effects.

Most of the above-mentioned studies were conducted on soils near active Zn or Cu smelters with ongoing emissions and only a few focused on long-abandoned contaminated sites (Juillot et al., 2011; Sivry et al., 2008; Sonke et al., 2008). Understanding the fate of historical contamination is challenging because it requires considering the effect of pedogenesis on metal cycling. It has been shown that pedogenetic processes alter Zn and Cu isotopic signatures through post-deposition fractionation (Juillot et al., 2011; Šillerová et al., 2017; Weiss et al., 2008) that with time, may compromise the identification of metal-sources. This post-deposition fractionation is caused by plant uptake of Zn and Cu depleting the soil in light isotopes (Aucour et al., 2015; Jouvin et al., 2012; Viers et al., 2007; Weinstein et al., 2011) and by metal-sorption to soil particles such as Fe-Mn oxides (Balistrieri et al., 2008; Bigalke et al., 2011; Bryan et al., 2015; Juillot et al., 2008;

84 Pokrovsky et al., 2008, 2005) or organic matter (Jouvin et al., 2009; Opfergelt et al., 2017) favoring
85 heavy isotope enrichments in soils.

86 In the 19th century, The Marseilleveyre Massif (Marseilles, France) was home to numerous
87 heavy industries, that have left derelict sites. While the area is now enclosed in the Calanques
88 National Park and is highly protected, it was found to be extensively impacted by these activities
89 (Daumalin and Raveux, 2016). The site of a former Pb-Ag smelter, located in the Escalette
90 Calanque, west of the massif, is particularly appropriate for studying the fate of a historical metal
91 contamination (Figure 1 and S1). It processed argentiferous galena ores from 1851 to 1925 by
92 pyrometallurgical processes and generated massive dumps of Pb and Zn-rich slags and
93 atmospheric emissions of highly metal-concentrated particles. Previous investigations (Affholder
94 et al., 2013; Testiati et al., 2013) showed that soil metal and metalloid concentrations (i.e. Pb, Sb,
95 Zn, Cd and Cu) in the immediate vicinity of the smelter are well above the values of the local
96 biogeochemical background (Austruy et al., 2016). However, no further investigations were
97 performed to evaluate the anthropogenic origin of the metals in more distant soils, or to identify a
98 possible vertical contamination along the soil profile.
99
100 In this study we combined elemental and isotopic Pb, Zn and Cu measurements with X-ray
101 Absorption Spectroscopy (XAS for Zn) analyses to: (i) characterize the isotopic signatures of the
102 pollution originating from the historical Escalette smelter ; (ii) determine whether the Cu
103 concentrations in soils result from galena ore processing or represent natural occurrences; (iii)
104 assess the extent of the vertical transfer of the contamination in a selection of soils of the Calanques
105 National Park located along a transect of increasing distance from the smelter.

106 The Escalette smelter did not process Cu. However, significant amounts of Cu can be present in
107 galena ores, as Cu can substitute into the crystal lattice e.g. (George et al., 2015). Thus, we decided
108 to use Cu isotopes to investigate whether traces of anthropogenic Cu could have been generated
109 during the smelting of galena and whether they could be detected in the surrounding soils.
110 Coupling Zn and Cu isotopes with Pb isotopes that are not affected by isotopic fractionation in
111 soils could help clarify the source of Zn and Cu if the signatures of these elements are too
112 compromised; this is especially the case in subsurface horizons where the pedogenetic processes
113 are the most effective. Furthermore, combining Zn isotopic signatures with Zn-speciation in soils
114 by XAS measurements could shed light on the possible alteration of Zn by pedogenetic processes
115 and/or on the transformation of Zn-bearing phases in soils. This method has proved to be efficient
116 for investigating the cycling of anthropogenic Zn in a soil-plant system (Aucour et al., 2015; Juillot
117 et al., 2011). Such a combination of analytical tools with multi-isotope systems was proposed by
118 Wiederhold (Wiederhold, 2015). To our knowledge, a combination of Pb, Zn and Cu isotopes has
119 been attempted in only one study dedicated to sourcing of urban aerosols (Souto-Oliveira et al.,
120 2018), and it has never been used for soil studies nor in combination with XAS measurements.
121

122 **Material and methods**

123 1. Smelter samples

124 The Escalette smelter produced PbO and $Ag_{(s)}$ by roasting PbS ores before casting under oxidic
125 conditions at ~ 1100°C, and separation of Pb and Ag. A detailed description of the
126 pyrometallurgical process can be found in Carlier et al. (2010). We collected eight slags resulting
127 from the smelting process along a solid reddish deposit located behind the smelter (Table S1 (c,
128 d)).

129 Grey coatings that had accumulated on the walls of the remaining creeping chimney (ca 300 m-
130 long) were sampled at both ends (i.e. close to the furnace and close to the exit) and in shielded
131 parts not exposed to external climatic conditions. Sampling of true emitted particles was
132 impossible since the smelter has been decommissioned. Considering that the chimney was not
133 equipped with any kind of particle-filtering system, we postulated that the chemical and isotopic
134 compositions of the sample collected at the top end of the chimney were the closest to those of the
135 metals emitted into the atmosphere and to those deposited onto the soils of the surrounding area.
136 Thus, it can be used as a proxy for the material deposited at the surface of the soils in the vicinity
137 of the smelter.
138
139 2. Soil samples
140 We selected five soil profiles along a 7-km NW-SE transect (Figure 1 and S1) of increasing
141 distance from the former smelter, and downwind of the dominant and most powerful wind (NW-
142 SE). These soils were developed on a marine limestone parent material of Cretaceous age, with
143 low metal concentrations (Text S1). The surrounding vegetation is typical of the Mediterranean
144 area (Affholder et al., 2013; Testiati et al., 2013).
145 These five soil profiles (S1, S2, S3, S4 and S5), labelled in order of increasing distance from the
146 smelter, were sampled and described according to the soil horizons. They were selected because
147 of their similar morphological and physico-chemical characteristics to ensure that different soil
148 properties and/or pedogenetic processes did not introduce any bias in the metal-distribution. They
149 are Colluviosols (Baize et al., 2009) or Leptosols (colluvic) (FAO, 2006) with a near neutral pH
150 of 8, an average organic carbon content of 37.3 g kg^{-1} and a mean $CaCO_3$ content of 247 g kg^{-1}. All
151 the profiles presented a loose and permeable stone/gravel layer of several centimeters resulting

152 from colluvial movements and set above the usual organic litter and A horizon. X-Ray Diffraction
153 results and physico-chemical characteristics of the samples, determined by the Laboratoire
154 d'Analyse des Sols (LAS) at Arras (INRA, France) are available in SI (Table S1a, S1b).
155
156 3. Total concentrations and isotopic analyses
157 Total concentrations and isotopic analyses were performed on the bulk soils, slags, and chimney
158 coatings. All soil samples were air dried and sieved to < 2mm. They were further crushed to a fine
159 powder in a mechanical agate mortar. For total metal concentrations and isotopic analyses, 150
160 mg of soil sample powder were weighed and calcined at 450°C for 4 hours to eliminate organic
161 matter, then dissolved using a mixture of concentrated HNO_3-HF-HCl at 130°C. Reagents were
162 either distilled acids (HNO_3, HCl) or Seastar© quality (HF). Slags and chimney coatings were
163 ground to a fine powder in an agate mortar and 50 mg of material was totally dissolved using 5 ml
164 of *aqua regia* at 130°C.
165 After digestion, total Pb, Zn and Cu concentrations were measured in solution using a PerkinElmer
166 Nexion 300X Q-ICP-MS.
167 For isotopic analyses, Cu, Zn and Pb were separated and purified using ion exchange
168 chromatography. Copper and Zn were separated and purified using an anionic resin (AG-MP1,
169 100-200 mesh, chloride form), following the procedure published in Maréchal et al. (1999). Lead
170 was separated using an anionic resin (AG1-X8, 100-200 mesh) following the procedure published
171 in (Fekiacova et al., 2007; Lugmair and Galer, 1992).
172 Measurements of Pb, Zn and Cu isotopic compositions were carried out at CEREGE using a
173 Thermo Fisher Scientific Neptune^{Plus} Multi-Collector Inductively Coupled Plasma Mass
174 Spectrometer (MC-ICP-MS).

^{208}Pb, ^{207}Pb, ^{206}Pb, ^{204}Pb isotopes corrected for instrumental blanks and mass bias fractionation were measured and are reported as isotope ratios for Pb and as δ notation (per-mil) for Zn (1) and Cu (2) relative to the IRMM-3702 Zn isotopic standard and the AES633 Cu isotopic standard.

(1) $\delta^{66}Zn = \left(\frac{\left(\frac{66Zn}{64Zn}\right)Sample}{\left(\frac{66Zn}{64Zn}\right)IRMM3702} - 1 \right) * 1000$

(2) $\delta^{65}Cu = \left(\frac{\left(\frac{65Cu}{63Cu}\right)Sample}{\left(\frac{65Cu}{63Cu}\right)AES633} - 1 \right) * 1000$

All data cited in the present paper are expressed relative to the IRMM-3702 standard for Zn and to the AES-633 standard for Cu. In order to compare our data with data from the literature expressed versus the no longer commercially available JMC-37049L (Zn) and NIST-976 (Cu) standards, the following equations were used (Sossi et al., 2015) .

$\delta^{66}Zn_{IRMM3702} = \delta^{66}Zn_{JMC37049L} - 0.3 \pm 0.02$ ‰

$\delta^{65}Cu_{AES633} = \delta^{65}Cu_{NIST976} + 0.01 \pm 0.05$ ‰

For $\delta^{66}Zn$ and $\delta^{65}Cu$, three measurements of each sample digestion were made and expressed as the average value of the three measurements; their repeatability is expressed as two standard deviations (2SD). Seven samples (i.e. all surface horizons of the soils from S1 to S5 and the chimney coatings, top and bottom) were duplicated by conducting a second sample preparation (digestion, column separation and analyses). Reproducibility of the replicated analyses was determined using ANOVA and presented as 2SD. Accuracy was controlled by processing the USGS reference material NOD-P-1 (Manganese nodule) with each batch of samples and reproducibility was calculated on the basis of 6 full replicates using the ANOVA procedure (Addinsoft, 2016). This material is well characterized for Zn (0.55 ±0.08‰; 0.48 ±0.09‰) and Cu (0.36 ±0.08‰; 0.47 ±0.08 isotopic compositions (Bigalke et al., 2010b; Chapman et al., 2006). The mean Zn (δ^{66}ZnIRMM-3702: 0.53 ±0.08 ‰) and Cu (δ^{65}CuAES-633: 0.45 ± 0.08‰) isotopic compositions of NODP1 obtained during this study agree with previously published data (Bigalke

198 et al., 2010b; Chapman et al., 2006). In addition to the Mn-nodule reference material, soil standards
199 (e.g. GBW07402 from the National Research Centre of Geoanalysis, Beijing, China, TILL-1 from
200 the CANMET Mining and Mineral Sciences Laboratories, Ottawa, Canada) were also processed
201 during this study. Their δ^{66}ZnIRMM-3702 and δ^{65}CuAES-633 isotopic compositions were
202 measured at 0.01 ±0.07‰. However, these results could not be compared to the literature as no
203 values have been published for these standards so far.
204 Copper and Zn chromatographic separation yields of processed samples were measured at 100%
205 ±10%. A further indicator of data quality is the strong correlation between δ^{66}Zn and δ^{67}Zn that
206 matches mass-dependent fractionation processes as specified in (Maréchal et al., 1999) (Figure
207 S2).
208 For Pb isotopes, one measurement was carried out per sample digestion. The repeatability of
209 analyses was estimated from multiple measurements of the bracketing standard NBS981 and is
210 expressed as two standard deviations (2SD).
211 More information on the procedure can be found in SI (Text S2).
212
213 4. EXAFS spectra acquisition and analysis
214 Zinc K-edge X-ray absorption spectra were recorded on samples of the chimney coatings (top)
215 and the surface horizons of S1 and S5 at the ESRF (Grenoble, France) on the BM30B (FAME)
216 beamline. Spectra were measured at liquid helium temperature and in fluorescence mode with a
217 30-element solid state Ge detector. Normalization and data reduction were performed according
218 to standard methods (Doelsch et al., 2006) using Athena software (Ravel and Newville, 2005). A
219 library of Zn reference compound spectra, described elsewhere (Formentini et al., 2017; Legros et

al., 2017) was used to identify Zn species in the samples. Details on the fitting procedure and results are given in SI (Text S3, Figure S3 (a, b) and Table S2).

Results and discussion

1. Characterization of slags and grey coatings originating from the former smelter

The Escalette smelter processed various sources of Pb-ores during its exploitation (Daumalin and Raveux, 2016). This variability of sources can impact the isotopic signatures of the volatile and residual phases formed during the smelter process. Moreover, high temperature processes are also known to induce large isotopic fractionation, particularly for Zn.

The Pb isotopic compositions of the sampled slags ranged from 2.0759 to 2.0999 and from 0.8371 to 0.8529, for $^{208}Pb/^{206}Pb$ and $^{207}Pb/^{206}Pb$ ratios, respectively (Table S1c). As Pb isotopes do not fractionate during the smelting of Pb-Zn ores (Cui and Wu, 2011; Shiel et al., 2010), this heterogeneity reflects the isotopic variability of the ores used during operation of the smelter (Daumalin and Raveux, 2016). By comparing historical reports of the smelter production and a published compilation of the Pb isotopic signature of the main ores (Stos-Gale et al., 1995), two Pb-Ag ores were identified as the origin of these slags: one from the Tuviois ore district (Sardinia, Italy) and the other from the Murcia Mazzaron district (Spain), that is consistent with the historical data found in (Daumalin and Raveux, 2016). The chimney recorded the isotopic signatures of all the processed ores, thus yielding an average Pb isotopic signature typical of the smelter emissions and characterized by values of 2.0924 and 0.8471, for $^{208}Pb/^{206}Pb$ and $^{207}Pb/^{206}Pb$, respectively (Table S1c).

Zinc and Cu isotopic compositions of slags and chimney coatings are presented in Figure 3 (b, c) and Table S1 (c, d). Zinc isotopic composition of the slags, ranged from -0.36 ±0.01 ‰ to -0.14

±0.05‰ (n=8), was heavier than that of the chimney coatings. Grey deposits collected in the chimney were enriched in light isotopes: -0.70 ±0.04 ‰ (top sample used as a proxy for the emitted particles, close to the chimney exit) and -0.26 ±0.09 ‰ (bottom, close to the furnace) that is consistent with previously published values for Zn or Cu smelters (Bigalke et al., 2010a; Mattielli et al., 2009; Sonke et al., 2008).

Previous studies demonstrated the enrichment of dust particles in light Zn isotopes resulting from Rayleigh-type isotope fractionation (Bigalke et al., 2010a; Mattielli et al., 2009; Shiel et al., 2010; Yin et al., 2016). This mechanism was also active during the Escalette smelting process and produced chimney deposits, enriched in light isotopes. Conversely, residual slags were enriched in heavy isotopes. Yet, the Rayleigh distillation did not produce slags with the same δ^{66}Zn value as we measured slight variations in the δ^{66}Zn values of these samples. These variations could reflect the isotopic variability of the galena ores used throughout 74 years of activity. This has also been suggested by other authors (Ochoa Gonzalez and Weiss, 2015) who found that in the combustion process of coal-fired power plants, Zn isotopic signatures of the by-products depended on those of the feed materials. Thus, Zn isotopic signatures of slags were first impacted by the isotopic variability of the parental ores and secondly by the Rayleigh distillation during the smelting.

The copper isotopic signature of the collected coatings varied from -0.22 ±0.04 ‰ (top) to -0.46 ±0.01 ‰ (bottom). Slags showed a larger range of δ^{65}Cu values than those observed for Zn isotopes, varying from -1.70 ±0.01‰ to 0.26 ±0.02 ‰ (n=8) (Figure 3c, Table S1c, Table S1d). δ^{65}Cu values of five out of eight slags were heavier (-0.11 ±0.1‰ to 0.26 ±0.02‰) than the chimney coating signature (-0.22 ±0.04 ‰ (top)). However, three slags displayed a lighter isotopic enrichment (-1.08 ±0.02 ‰; -1.70 ±0.01 ‰; -1.34 ±0.03 ‰) than the chimney coatings (Table S1d).

Previous studies showed that Cu is not affected by Rayleigh distillation (Bigalke et al., 2010a; Gale et al., 1999) even in Cu smelters, since the Cu isotopic signatures of ash and slags are similar. The volatilization temperature of Cu is higher than that of Zn ($T°_{volatilization}$: 2595°C and 907°C, respectively). The smelting process temperature at the Escalette smelter varied between 1000 and 1150°C (Carlier et al., 2010), thus allowing volatilization for Zn, but not for Cu. We thus hypothesize that the Cu isotopic heterogeneity found in slags mainly resulted from inputs of various galena-ores rather than from an isotopic distillation. No data are available for δ^{65}Cu values in galena ores to confirm this hypothesis, but Cu-S bearing ores (i.e. chalcopyrite and enargite), that are chemically close to the Pb-S (galena) ores processed by the smelter, display δ^{65}Cu values ranging from -1% to 1% (Mathur et al., 2009) that fit our measurements.

We measured different isotopic compositions at the bottom and the top of the chimney (Figure 3b, Table S1c). Copper and Zn isotopic signatures of the bottom sample (δ^{65}Cu: -0.46 ±0.01 ‰; δ^{66}Zn: -0.26 ±0.09 ‰) were close to those measured for slags while the top sample was enriched in light Zn isotope (-0.70 ±0.04 ‰), and heavy Cu isotope (-0.22 ±0.04 ‰). We propose therefore that the Cu and Zn isotopic signatures of the chimney bottom sample are close to those of the processed ores like the slags; while in the top sample, isotopic signatures were affected by Rayleigh distillation (for Zn) and equilibrium fractionation (for Cu) that occurred during transport in the vapor phase. A decrease in the plume temperature and condensation of particles during the vapor phase travelling as observed by (Ochoa Gonzalez and Weiss, 2015) in bottom and flying ash samples from a coal power plant could explain the differences in metal concentrations between the two extremities of the chimney. Like other smelters in the area at that time, the Escalette smelter is characterized by a long sub-horizontal conduit, built on the ground, and creeping up the hill along the ridge rather than by the short, vertical chimneys as found in modern smelters. Thus,

interactions of Zn and Cu during transport in the vapor phase were maximized causing an enrichment in light Zn isotope and an enrichment in heavy Cu isotope (Balistrieri et al., 2008; Pokrovsky et al., 2008).

2. Assessing the extent of the soil contamination

Elemental concentrations: highlighting soil surface contamination.

Trace metal concentrations in the soil profiles (Figure 2a, b, c and Table S1c) were studied to determine the horizontal extent of metal contamination in the vicinity of the Escalette smelter. Surface horizons of the S1, S2, and S3 profiles were clearly affected by atmospheric deposition of metal-rich particles with Pb and Zn concentrations decreasing with increasing distance from the smelter and metal levels in the S1 A horizon up to 121x (Pb) and 14x (Zn) those found in the deep horizon of the more distant soil (S5 C) (table S1c).

For all the studied soils, the surface horizons showed higher Pb, Zn, and Cu concentrations than deeper horizons except for S5 that had the lowest trace metal concentrations in the A horizons. All Zn and Pb concentrations were well above the values measured in five unpolluted local soils developed on calcareous parent materials (Austruy et al., 2016), both for the A topsoil (up to 22-fold for Zn and 39-fold for Pb) and for the subsoils (up to 3-fold for Zn and Pb). In S5, Zn concentrations were higher than those for natural calcareous soils in both surface (27 to 64 mg kg^{-1} (Austruy et al., 2016)) and deep horizons (19 to 59 mg kg^{-1} (Austruy et al., 2016)). However, Pb concentrations were lower than those estimated by (Austruy et al., 2016) both for surface (20 to 78 mg kg^{-1}) and deep horizons (9 to 42 mg kg^{-1}).

In all soils, Cu concentrations were low and close to geogenic values ranging from 4 mg kg^{-1} to 17 mg kg^{-1} (Austruy et al., 2016) compared to Zn and Pb (Figure 2c). However, S1 displayed

311 concentrations ~2.5x higher than S5 indicating a small potential contamination by smelter
312 emissions. Soils displayed more homogenous Cu concentrations with a smaller depth-induced
313 decrease, that was most likely due to initially lower Cu concentrations in the parental limestone
314 and to a low concentration in the source galena, thus in smelter emissions.

315 Although S2 was closer to the smelter than S3 (Figure S1b), Zn, Pb, and Cu concentrations were
316 lower. This could be related to the fact that S2 was obscured from direct line of sight by a
317 calcareous cliff that may have limited the deposition of metal-bearing airborne particles even with
318 NNW winds that can reach up to 110 km h^{-1}.

319 High trace metal concentrations in surface horizons decreasing with depth are similar to patterns
320 observed in uncontaminated soils (Legros, 2007). Furthermore, higher trace metal concentrations
321 in deep horizons compared to other soils in the area could originate from a higher pedogeochemical
322 background. Local variations in the natural pedo-geochemical background can be determined from
323 the relationship between total Fe and the trace metals and can provide information about a potential
324 trace metal contamination (Baize and Sterckeman, 2001). In our soils, the relationship between
325 total Fe and trace metals made it possible to distinguish between (i) a group of deep horizons
326 having low trace metal concentrations and (ii) a group of surface horizons, with a high trace metal
327 content for relatively low Fe concentrations. This approach revealed the horizontal extent of trace
328 metal contamination of surface horizons in the Escalette area, but did not inform on the potential
329 transfers of anthropogenic metals down the profiles and/or on the source contributions.

330

331 **3. Isotopic signatures: tracing the smelter contamination in soil profiles**

332 3.1 Lead

The surface horizons of all profiles showed Pb isotopic compositions similar to those of the chimney coatings and the slags, indicating that lead contamination originated from smelter emissions. In a $^{208}Pb/^{206}Pb$ vs $^{207}Pb/^{206}Pb$ plot (Figure 4a), soils and chimney coatings lay along a linear trend corresponding to a mixing line between a radiogenic end-member (i.e. the emitted anthropogenic Pb), and an uncontaminated end-member characterized by a lower radiogenic Pb signature (i.e. the local pedogeochemical background) found in the S5 deepest horizon.

Lead isotopic ratios of the slags plotted out this $^{208}Pb/^{206}Pb$ vs $^{207}Pb/^{206}Pb$ mixing line (Figure 4a) and demonstrate that slag-generated dust did not contribute to the soil contamination. Moreover, considering the local topography and the fact that these slags appeared as a solid unaltered material, it is unlikely that slag-related dust contaminated soils located at the top of the slopes. This observation supports the hypothesis that Pb contamination in soils was solely caused by the metal-rich particles emitted by the smelter. Furthermore, the chimney signature reflects the average composition of all the isotopic compositions of galena ores processed over time (Figure 3a and Figure 4a).

The limited variation of $^{208}Pb^{206}Pb$ ratios with depth (Figure 3a) or the soil profile distribution on the mixing line (Figure 4a), indicates that (i) Pb contamination affected all soils from S1 to S5 (ii) Pb concentrations in soils resulted from two lead sources and (iii), anthropogenic Pb was transferred towards depth.

In Figure 4a the S5 A horizon lies slightly off the mixing line, indicating that this sample received a contribution from another lead source other than the smelter, e.g. urban aerosols or modern industrial sources. Three-component mixing for this sample can also be identified in a $^{208}Pb/^{204}Pb$ vs $^{206}Pb/^{204}Pb$ plot (Figure 4b) as suggested by (Ellam, 2010). This source was not observed in other soils because of the dominant lead signature from the smelter particles. We hypothesize that this

356 source may be representative of the atmospheric aerosols emitted by the combustion of fossil
357 energy (i.e. road traffic in Marseilles) after the closing of the smelter.
358 Reconstruction of the lead isotopic signature of French (northern and southern) atmospheric
359 aerosols since the 1980s, based on previously published data (Luck and Ben Othman, 2002b;
360 Maring et al., 1987; Véron et al., 1999), produced a mixing line ($r^2 = 0.95$; p value $=1.40E^{-19}$) that
361 did not intersect our S5 A horizon sample, but instead drove it away from the two end-member
362 mixture (Figure S4).
363 3.2 Zinc

364 Zinc isotopic signatures of the smelter samples (chimney) and the soil samples were different
365 (Figure 3b). The impact of light Zn-rich particles originating from the smelter could nonetheless
366 be detected in the surface horizons.
367 Soil surface horizons from S1 to S4 showed δ^{66}Zn values ranging from -0.24 ±0.05 ‰ to -0.43
368 ±0.06‰ (Table S1c, Figure 3b). The surface horizon of S5 had the heaviest Zn isotopic signature
369 (-0.14 ±0.06‰ Figure 3b), that remained constant along the entire profile.
370 Isotope studies carried out on peat core sediments (Sonke et al., 2008) or on soils collected near a
371 Zn or Cu smelter (Bigalke et al., 2010a; Juillot et al., 2011), revealed a similar enrichment in light
372 isotopes in the sediment/soil surface samples compared to those measured in the chimney stacks
373 or smelter dust. However, these studies also noted discrepancies between Zn isotopic compositions
374 of the smelter emissions and those of the sediment/soils. The discrepancy was explained by either
375 mixing of the ash/dust signal with other emissions from different subunits of the smelter (Bigalke
376 et al., 2010a; Juillot et al., 2011) or by post-depositional fractionation (Juillot et al., 2011) that
377 induced direct heavy enrichment in soils by Zn-sorption onto oxides and OM (Bryan et al., 2015;
378 Guinoiseau et al., 2016; Jouvin et al., 2009; Juillot et al., 2008; Pokrovsky et al., 2005) or depletion

in light isotopes by plant uptake (Aucour et al., 2015; Jouvin et al., 2012; Viers et al., 2007). This hypothesis was supported by other authors (Mattielli et al., 2009) who found a perfect match between Zn isotopic composition of the chimney dust and particles collected on dry plate rather than environmental (soil) samples, thus preventing any interactions with soil particles or plant uptake. Thus, the enrichment in heavy Zn isotopes in surface horizons of the studied soils could be explained by the direct (i.e. sorption) or the indirect (i.e. plant uptake) effect of post-deposition fractionation processes.

Soil profiles S1, S2, and S3 displayed isotopic variations with depth, up to $\Delta^{66}Zn_{\text{S3 A horizon-S3 S horizon}}$ = 0.21 ‰ in S3 soil, and an increase in the $\delta^{66}Zn$ values down to ~ 0.2 m (Figure 3b). $\delta^{66}Zn$ values of the deepest horizons of S1, S2, S3, and S4 were close to the isotopic signature of S5 and indicated that Zn contamination may have been limited at depth. Homogeneous Zn concentrations and $\delta^{66}Zn$ values in the S5 profile were (i) clearly distinct from those of the chimney and of the other soils, and (ii) fell within the range of previously published values for non-contaminated soils or continental rock parental material (-0.19 to 0.06 ‰) (Juillot et al., 2011; Pichat et al., 2003; Sonke et al., 2008; Wilkinson et al., 2005). Thus, we propose that the $\delta^{66}Zn$ value in S5 (~ -0.16 ‰) reflects the Zn isotopic signature of the local uncontaminated weathered parent material for the studied soil.

3.3 Copper

Given the proximity of S1, S2, and S3 to the chimney, a significant contribution of particle deposition on the Cu isotopic signatures in these soils was expected, especially for S1 where the Cu concentration was slightly higher in the A horizon (Figure 2c). However, (i) Cu isotopic

signatures in the A horizons of S1 and S5 are similar (Figure 3c), and (ii) they did not reveal any similarities between soil surface and chimney coating unlike for Pb and Zn isotopes (Figure 3c).

Except for S4, all profiles showed a similar vertical distribution, with an increasing light isotope contribution at depth as observed in (Bigalke et al., 2011; Mihaljevič et al., 2018) for natural soils. δ^{65}Cu values in deep horizons ranged from -0.30 ±0.04 ‰ to -0.73 ±0.03 ‰, values that are within the range of δ^{65}Cu values measured in unpolluted soils, (-0.9 to 0.45 ‰ (Bigalke et al., 2011; Fekiacova et al., 2015; Kříbek et al., 2018).

We conclude that anthropogenic inputs of Cu from the smelter were negligible and observed Cu fractionation in the soil profiles was produced by pedogenetic processes. Two major processes are known to impact natural Cu isotopic signatures in soils: plant recycling (Jouvin et al., 2012; Weinstein et al., 2011) and interactions with solid mineral particles and/or solid organic matter (Balistrieri et al., 2008; Bigalke et al., 2011; Pokrovsky et al., 2008). These interactions cause direct (preferential sorption) and indirect (depletion of light isotopes by plant uptake) heavy isotope enrichment in soils. We propose that Cu concentrations in the soils were inherited from the parent material and higher Cu concentrations in the surface horizons resulted from Cu complexation to the organic matter. A ^{65}Cu enrichment observed in the surface horizons corroborates this hypothesis.

4. Long-term fate of anthropogenic Pb and Zn in soils.

Emissions from the Escalette smelter and contamination started 167 years ago and lasted 74 years. Thus, the Escalette site provides a unique place to unravel the long-term fate of anthropogenic Pb and Zn in terms of remobilization/redistribution within the impacted soils.

4.1 Lead

The limited vertical variation of $^{208}Pb/^{206}Pb$ ratios (Figure 3a) indicated that anthropogenic Pb, characterized by a high $^{208}Pb/^{206}Pb$ ratio (Table S1c), was transferred to depth from S1 to S4. Soluble transport of Pb in carbonated soil is limited because of the preferential precipitation of Pb as carbonates (cerussite, hydrocerussite or pyromorphite) at pH > 5.2 (Gee et al., 1997; Yanful et al., 1988). The pH of all studied soils ranged from 7.9 to 8.3 suggesting possible Pb carbonate precipitation, although no Pb carbonate was detected by XRD (probably due to concentrations below the detection limit). Considering the high distribution coefficient (*K*d) of Pb for OM and Fe-oxides in poorly developed carbonated soils (Dumat et al., 2001; Lafuente et al., 2008), Pb is likely to occur as complexes with organic matter and soil minerals in the surface horizons of the studied soils. We hypothesized that Pb redistribution by colluvial processes could explain the results. However, erosion of upslope-contaminated-material and accumulation of eroded material downslope should be reflected by (i) Pb and Zn concentration peaks in subsurface horizons of downslope profiles, and (ii) abrupt changes in the Zn isotopic signatures of intermediate horizons toward light values caused by the integration of smelter-derived particles characterized by light $\delta^{66}Zn$ values. Since none of these effects were observed, we concluded that colluvial processes were not responsible for anthropogenic Pb migration.

Using a mixing model between two end-members (Figure 4a and 5) represented by the deepest horizon of S5 (C) and the chimney coating (top) and based on the calculation proposed by (Phillips and Gregg, 2003), we can estimate the contribution of anthropogenic Pb to the total Pb pool in soils. We found that Pb-rich particles from the smelter (Figure 5, Table S3) account for at least 91% of the total Pb pool measured in soil surface horizons from S1 to S4. The deepest soil horizons

446 show the same trend with an anthropogenic Pb contribution estimated between 65-78% from S1
447 to S4.

448 The A horizon of S5 plotted out of the mixing line (Figure 4a and Figure 5) and the $^{208}Pb/^{204}Pb$ vs
449 $^{206}Pb/^{204}Pb$ isotope plot confirmed the contribution of a third source of Pb in this sample (Figure 4b).
450 Thus, we used the Isosource program (Phillips and Gregg, 2003), provided by the Environmental
451 Protection Agency, to calculate contributions of different Pb sources in a three end-member system
452 (smelter, geogenic, atmospheric). The third Pb source considered in the system was urban aerosol,
453 with values of $^{208}Pb/^{206}Pb = 2.1367$ and $^{207}Pb/^{206}Pb = 0.8944$, approximated by the Pb signature of
454 Marseilles aerosols in 1987 (Maring et al., 1987).

455 According to these calculations, in S5 (the most distant soil from the smelter), the contribution of
456 smelter-related anthropogenic Pb was best estimated at 39%, geogenic Pb at 42% and atmospheric
457 Pb at 19%. The distributions of all possible contributions that satisfied the isotopic mass balance
458 calculations are presented in (Figure S5, Table S3).

459 This observation indicated that some Pb-rich particles from the smelter travelled up to 7 km SE.
460 However, because of a lower concentration of the smelter-derived particles, Pb isotopic signature
461 of S5 was significantly disturbed by inputs of atmospheric particles when smelter emissions
462 stopped in 1925. At the other sites, the impact of atmospheric particles was not observable, most
463 likely due to a higher content of smelter-derived particles.

464 The anthropogenic Pb contribution to total Pb decreased progressively with depth in all soils,
465 excluding the impact of colluvial processes on Pb distribution in soils as stated above. Based on
466 soil thickness, we calculated Pb penetration rates in soils ranging from 0.27 cm $year^{-1}$ (S1 soil) to
467 0.47 cm $year^{-1}$ (S3 soil) for a lower limit (i.e. calculated since the opening of the smelter, 167 years
468 ago) or 0.48 cm $year^{-1}$ to 0.85 cm $year^{-1}$ in the same soils for the upper limit (i.e. calculated since

469 the decommissioning of the smelter, 93 years ago). As Pb migration has been found to be facilitated
470 by colloidal transport in contaminated soil (Amrhein et al., 1993; Denaix et al., 2001; Grolimund
471 et al., 1996; Grolimund and Borkovec, 2005; Kretzschmar and Schafer, 2005) and because of both
472 low Pb concentrations in the < 0.2 μm soluble phase (Gelly et al. *in prep*) and low soil density, we
473 propose that in the soils, this transfer occurred in the particulate form. Furthermore, metal
474 migration could have been enhanced by bioturbation (e.g. (Sterckeman et al., 2000), but we did
475 not observe any evidence of significant worm activity to support this hypothesis.
476
477 4.2 Zinc
478 Zinc contamination was detected using Zn isotopes in all soils except S5. However, vertical
479 variations in δ^{66}Zn values indicated that Zn mobility was different from that observed for Pb.
480 Smelter-related Zn, characterized by light δ^{66}Zn values (Figure 3b), accumulated within the A and
481 A/C horizons. However, the observed shift towards heavier signatures in the studied soils
482 demonstrates that another process modified the initial anthropogenic Zn signature. This shift could
483 be attributed to (i) Zn adsorption or precipitation on organic matter and Al-Fe-Mn oxides
484 (Balistrieri et al., 2008; Juillot et al., 2008; Pokrovsky et al., 2005), that would promote heavy
485 isotope complexes, or to (ii) plant uptake, that would deplete soil in light isotopes, thus enriching
486 it in heavy ones (Aucour et al., 2015; Jouvin et al., 2012; Viers et al., 2007).
487 EXAFS results support the hypothesis of the transformation of anthropogenic Zn. In S1, Zn
488 speciation could not be fitted by a simple combination of the chimney (anthropogenic contribution)
489 and S5 compositions (natural contribution), indicating a change in the smelter-related Zn
490 speciation after deposition onto the soil (Figure S3b). EXAFS results highlighted the precipitation
491 of a Zn-layered double hydroxide (Zn-LDH) phase which was dominant (~77%, Table S2) in S1

topsoil, while in the S5 soil, Zn was mostly sorbed onto Fe and Mn oxides (Table S2). Zn-LDH precipitates have been identified as markers of Zn contamination in calcareous soils (Jacquat et al., 2008; Juillot et al., 2003; Voegelin et al., 2011) or other contaminated soils (Aucour et al., 2015; Voegelin et al., 2005). Zn-LDH precipitation occurs once all sorption sites have been saturated (Luxton et al., 2013) and is kinetically favored over precipitation of Zn-phyllosilicates, although these precipitates are also thermodynamically stable (Voegelin et al., 2005). The availability of Al and Si (Jacquat et al., 2008; Voegelin et al., 2005) and increasing Zn concentrations in soils seem to play a major role in the formation of Zn-LDH. No occurrences of Zn-LDH in Pb and/or Zn smelter exhausts have been reported in the literature. Similarly, we did not detect these compounds in the Escalette chimney (Table S2), most likely indicating unfavorable physico-chemical conditions in the chimney (e.g. more acidic pH).

Thus, Zn-LDH formation was considered to have contributed to (i) precipitation of smelter-related Zn in the S1 surface horizon, and (ii) alteration of the Zn isotopic signatures of the emitted particles by favoring heavy isotope complexes. Owing to the similarity in the Zn isotopic signature of the A horizons in S1 to S4, the same process may have occurred in all studied soils.

The mixing model calculated for Zn (like the model calculated for Pb) did not show any progressive mixing between the two end-members, but rather highlighted two Zn pools. One pool was represented by the surface horizons of soils from S1 to S4, the second one was represented by the deepest horizons of these soils and by the entire S5 profile (Figure 6). Separation of the Zn pools confirmed that anthropogenic Zn accumulated in surface horizons and that precipitation of the Zn-LDH prevented leaching of Zn towards deeper horizons. Consequently, at depth, Zn is considered to be of geogenic origin (inherited from the parental limestone).

514 Zinc isotopes confirmed that few Zn-rich particles reached S5 as their impact was not recorded by
515 the δ^{66}Zn values, probably because anthropogenic Zn was incorporated in soils through pedogenetic
516 processes as illustrated by EXAFS analyses (Table S2).
517
518 Conclusion
519 We used isotopic analyses to shed light on the behavior and transfer in soils of Pb, Zn, and Cu
520 emitted simultaneously from the Escalette smelter, for 93 years. In contrast to Pb and Zn, Cu
521 isotopes showed no evidence of Cu contamination of the soils in the vicinity of the Escalette
522 smelter.
523 We recovered traces of smelter emissions in the soil surface (Zn-Pb) up to 7 km away from the
524 smelter and at depth (Pb). The vertical mobility of anthropogenic Pb contrasts with previously
525 published data on calcareous soils where Pb was immobilized in surface horizons.
526 In contrast, immobilization of smelter-related Zn within the surface horizons was documented
527 by the shift in δ^{66}Zn values in soils compared to those of the chimney coatings, representing the
528 proxy used for the isotopic signatures of the emitted particles. This is explained by the precipitation
529 of Zn-LDH, typical of Zn-rich environments with near-neutral to slightly basic pH. This form of
530 Zn was different from those observed in the chimney coatings and in S5, indicating that (i)
531 speciation of Zn emitted from the smelter changed after deposition, altering Zn isotopic signatures,
532 and (ii) fewer Zn-rich particles reached S5 and were included in the biogeochemical cycle of Zn
533 through pedogenetic processes.
534 However, the role of vegetation in the anthropogenic Zn cycling at this site needs to be
535 deciphered in future studies. Particularly, *in natura* isotopic measurements could shed light on how
536 the vegetation adapts to anthropogenic metals and incorporates them into its biogeochemical cycle.

This work underlines the complementarity of elemental, isotopic, and speciation analyses for tracing and unravelling the fate of historical multi-metal contamination in soils by providing a complementary set of data that highlights the distinctive behavior of trace metals originating from a common industrial source.

Acknowledgement

The authors wish to thank A. Veron for useful insights on Pb isotopes, D. Borschneck for support on XRD measurements, B. Angeletti for Q-ICP-MS analyses, J. Balesdent for ^{13}C analyses and P. Höhener for critically reading the manuscript. We thank the anonymous reviewers for their constructive reviews that helped improve the manuscript. This work was supported by the following projects: Agence Nationale pour la Recherche (ANR, France) project EQUIPEX ASTER-CEREGE, Pari Scientifique EA-INRA (COMETICS), ANR project MARSECO (CES018-2008), Labex DRIIHM, French Program "Investissements d'avenir" (ANR-11-LABX-0010). We acknowledge the European Synchrotron Radiation Facility (ESRF) for the provision of synchrotron beam time.

References

Addinsoft, 2016. XLSTAT 2016: Data Analysis and Statistical Solution for Microsoft Excel.

Affholder, M.-C., Prudent, P., Masotti, V., Coulomb, B., Rabier, J., Nguyen-The, B., Laffont-Schwob, I., 2013. Transfer of metals and metalloids from soil to shoots in wild rosemary (Rosmarinus officinalis L.) growing on a former lead smelter site: Human exposure risk. Sci. Total Environ. 454–455, 219–229. https://doi.org/10.1016/j.scitotenv.2013.02.086

Amrhein, C., Mosher, P.A., Strong, J.E., 1993. Colloid-Assisted Transport of Trace Metals in Roadside Soils Receiving Deicing Salts. Soil Sci. Soc. Am. J. 57, 1212. https://doi.org/10.2136/sssaj1993.03615995005700050009x

Araújo, D.F., Machado, W., Weiss, D., Mulholland, D.S., Garnier, J., Souto-Oliveira, C.E., Babinski, M., 2018. Zinc isotopes as tracers of anthropogenic sources and biogeochemical

processes in contaminated mangroves. Appl. Geochem. 95, 25–32. https://doi.org/10.1016/j.apgeochem.2018.05.008
Aucour, A.-M., Bedell, J.-P., Queyron, M., Magnin, V., Testemale, D., Sarret, G., 2015. Dynamics of Zn in an urban wetland soil–plant system: Coupling isotopic and EXAFS approaches. Geochim. Cosmochim. Acta 160, 55–69. https://doi.org/10.1016/j.gca.2015.03.040
Austruy, A., Dron, J., Charbonnier, E., Babaguela, N., Miche, H., Keller, C., Chamaret, P., 2016. Teneurs naturelles et apports anthropiques en éléments traces dans les sols à l'ouest de l'étang de Berre. Etude Gest. Sols 18.
Baize, D., Girard, M.-C., others, 2009. Référentiel pédologique 2008. Quae.
Baize, D., Sterckeman, T., 2001. Of the necessity of knowledge of the natural pedo-geochemical background content in the evaluation of the contamination of soils by trace elements. Sci. Total Environ. 264, 127–139. https://doi.org/10.1016/S0048-9697(00)00615-X
Balistrieri, L.S., Borrok, D.M., Wanty, R.B., Ridley, W.I., 2008. Fractionation of Cu and Zn isotopes during adsorption onto amorphous Fe(III) oxyhydroxide: Experimental mixing of acid rock drainage and ambient river water. Geochim. Cosmochim. Acta 72, 311–328. https://doi.org/10.1016/j.gca.2007.11.013
Bigalke, M., Weyer, S., Kobza, J., Wilcke, W., 2010a. Stable Cu and Zn isotope ratios as tracers of sources and transport of Cu and Zn in contaminated soil. Geochim. Cosmochim. Acta 74, 6801–6813. https://doi.org/10.1016/j.gca.2010.08.044
Bigalke, M., Weyer, S., Kobza, J., Wilcke, W., 2010b. Stable Cu and Zn isotope ratios as tracers of sources and transport of Cu and Zn in contaminated soil. Geochim. Cosmochim. Acta 74, 6801–6813. https://doi.org/10.1016/j.gca.2010.08.044
Bigalke, M., Weyer, S., Wilcke, W., 2011. Stable Cu isotope fractionation in soils during oxic weathering and podzolization. Geochim. Cosmochim. Acta 75, 3119–3134. https://doi.org/10.1016/j.gca.2011.03.005
Borrok, D.M., Wanty, R.B., Ian Ridley, W., Lamothe, P.J., Kimball, B.A., Verplanck, P.L., Runkel, R.L., 2009. Application of iron and zinc isotopes to track the sources and mechanisms of metal loading in a mountain watershed. Appl. Geochem. 24, 1270–1277. https://doi.org/10.1016/j.apgeochem.2009.03.010
Bryan, A.L., Dong, S., Wilkes, E.B., Wasylenki, L.E., 2015. Zinc isotope fractionation during adsorption onto Mn oxyhydroxide at low and high ionic strength. Geochim. Cosmochim. Acta 157, 182–197. https://doi.org/10.1016/j.gca.2015.01.026
Carlier, C.M.-L., Ploquin, A., Fluck, P., 2010. Apport de la géochimie et de la pétrologie à la connaissance de la métallurgie primaire du plomb argentifère au Moyen Âge: Les exemples du Mont Lozère (Cévennes) et de Pfaffenloch (Vosges). ArchéoSciences 159–176. https://doi.org/10.4000/archeosciences.2728
Chapman, J.B., Mason, T.F.D., Weiss, D.J., Coles, B.J., Wilkinson, J.J., 2006. Chemical Separation and Isotopic Variations of Cu and Zn From Five Geological Reference Materials. Geostand. Geoanalytical Res. 30, 5–16. https://doi.org/10.1111/j.1751-908X.2006.tb00907.x
Cloquet, C., Carignan, J., Libourel, G., Sterckeman, T., Perdrix, E., 2006. Tracing Source Pollution in Soils Using Cadmium and Lead Isotopes. Environ. Sci. Technol. 40, 2525–2530. https://doi.org/10.1021/es052232+
Cui, J., Wu, X., 2011. AN EXPERIMENTAL INVESTIGATION ON LEAD ISOTOPIC FRACTIONATION DURING METALLURGICAL PROCESSES: Lead isotopic

fractionation during metallurgical processes. Archaeometry 53, 205–214. https://doi.org/10.1111/j.1475-4754.2010.00548.x
Daumalin, X., Raveux, O., 2016. A region scarred by pollution, in: Xavier Daumalin, I.L.-S. (dir. . (Ed.), Es Calanques Industrielles de Marseille et Leurs Pollutions. Une Histoire Au Présent. REF.2C éditions, pp. 131–203.
Denaix, L., Semlali, R.M., Douay, F., 2001. Dissolved and colloidal transport of Cd, Pb, and Zn in a silt loam soil a□ected by atmospheric industrial deposition. Environ. Pollut. 10.
Desenfant, F., Veron, A.J., Camoin, G.F., Nyberg, J., 2006. Reconstruction of pollutant lead invasion into the tropical North Atlantic during the twentieth century. Coral Reefs 25, 473–484. https://doi.org/10.1007/s00338-006-0113-x
Doelsch, E., Masion, A., Borschneck, D., Hazemann, J.-L., Saint Macary, H., Bottero, J.-Y., Rose, J., Basile-Doelsch, I., 2006. New Combination of EXAFS Spectroscopy and Density Fractionation for the Speciation of Chromium within an Andosol. Environ. Sci. Technol. 40, 7602–7608. https://doi.org/10.1021/es060906q
Dumat, C., Chiquet, A., Gooddy, D., Aubry, E., Morin, G., Juillot, F., Benedetti, M.F., 2001. Metal ion geochemistry in smelter impacted soils and soil solutions. Bull. Société Géologique Fr. 172, 539–548. https://doi.org/10.2113/172.5.539
Ellam, R.M., 2010. The graphical presentation of lead isotope data for environmental source apportionment. Sci. Total Environ. 408, 3490–3492. https://doi.org/10.1016/j.scitotenv.2010.03.037
Erel, Y., Veron, A., Halicz, L., 1997. Tracing the transport of anthropogenic lead in the atmosphere and in soils using isotopic ratios. Geochim. Cosmochim. Acta 61, 4495–4505. https://doi.org/10.1016/S0016-7037(97)00353-0
FAO (Ed.), 2006. World reference base for soil resources 2006: a framework for international classification, correlation and communication, World soil resources reports. FAO, Rome.
Fekiacova, Z., Abouchami, W., Galer, S.J.G., Garcia, M.O., Hofmann, A.W., 2007. Origin and temporal evolution of Ko‘olau Volcano, Hawai‘i: Inferences from isotope data on the Ko‘olau Scientific Drilling Project (KSDP), the Honolulu Volcanics and ODP Site 843. Earth Planet. Sci. Lett. 261, 65–83. https://doi.org/10.1016/j.epsl.2007.06.005
Fekiacova, Z., Cornu, S., Pichat, S., 2015. Tracing contamination sources in soils with Cu and Zn isotopic ratios. Sci. Total Environ. 517, 96–105. https://doi.org/10.1016/j.scitotenv.2015.02.046
Formentini, T.A., Legros, S., Fernandes, C.V.S., Pinheiro, A., Le Bars, M., Levard, C., Mallmann, F.J.K., da Veiga, M., Doelsch, E., 2017. Radical change of Zn speciation in pig slurry amended soil: Key role of nano-sized sulfide particles. Environ. Pollut. 222, 495–503. https://doi.org/10.1016/j.envpol.2016.11.056
Gale, N.., Woodhead, A.., Stos-Gale, Z.., Walder, A., Bowen, I., 1999. Natural variations detected in the isotopic composition of copper: possible applications to archaeology and geochemistry. Int. J. Mass Spectrom. 184, 1–9. https://doi.org/10.1016/S1387-3806(98)14294-X
Gee, C., Ramsey, M.H., Maskall, J., Thornton, I., 1997. Mineralogy and weathering processes in historical smelting slags and their effect on the mobilisation of lead. J. Geochem. Explor. 58, 249–257. https://doi.org/10.1016/S0375-6742(96)00062-3
George, L., Cook, N.J., Ciobanu, C.L., Wade, B.P., 2015. Trace and minor elements in galena: A reconnaissance LA-ICP-MS study. Am. Mineral. 100, 548–569. https://doi.org/10.2138/am-2015-4862

655 Grolimund, D., Borkovec, M., 2005. Colloid-Facilitated Transport of Strongly Sorbing
656 Contaminants in Natural Porous Media: Mathematical Modeling and Laboratory Column
657 Experiments †. Environ. Sci. Technol. 39, 6378–6386. https://doi.org/10.1021/es050207y
658 Grolimund, D., Borkovec, M., Barmettler, K., Sticher, H., 1996. Colloid-Facilitated Transport of
659 Strongly Sorbing Contaminants in Natural Porous Media: A Laboratory Column Study.
660 Environ. Sci. Technol. 30, 3118–3123. https://doi.org/10.1021/es960246x
661 Guinoiseau, D., Gélabert, A., Moureau, J., Louvat, P., Benedetti, M.F., 2016. Zn Isotope
662 Fractionation during Sorption onto Kaolinite. Environ. Sci. Technol. 50, 1844–1852.
663 https://doi.org/10.1021/acs.est.5b05347
664 Hamelin, B., Ferrand, J.L., Alleman, L., Nicolas, E., Veron, A., 1997. Isotopic evidence of
665 pollutant lead transport from North America to the subtropical North Atlantic gyre.
666 Geochim. Cosmochim. Acta 61, 4423–4428. https://doi.org/10.1016/S0016-
667 7037(97)00242-1
668 Jacquat, O., Voegelin, A., Villard, A., Marcus, M.A., Kretzschmar, R., 2008. Formation of Zn-
669 rich phyllosilicate, Zn-layered double hydroxide and hydrozincite in contaminated
670 calcareous soils. Geochim. Cosmochim. Acta 72, 5037–5054.
671 https://doi.org/10.1016/j.gca.2008.07.024
672 Jeon, S., Kwon, M.J., Yang, J., Lee, S., 2017. Identifying the source of Zn in soils around a Zn
673 smelter using Pb isotope ratios and mineralogical analysis. Sci. Total Environ. 601–602,
674 66–72. https://doi.org/10.1016/j.scitotenv.2017.05.181
675 Jouvin, D., Louvat, P., Juillot, F., Maréchal, C.N., Benedetti, M.F., 2009. Zinc Isotopic
676 Fractionation: Why Organic Matters. Environ. Sci. Technol. 43, 5747–5754.
677 https://doi.org/10.1021/es803012e
678 Jouvin, D., Weiss, D.J., Mason, T.F.M., Bravin, M.N., Louvat, P., Zhao, F., Ferec, F., Hinsinger,
679 P., Benedetti, M.F., 2012. Stable Isotopes of Cu and Zn in Higher Plants: Evidence for Cu
680 Reduction at the Root Surface and Two Conceptual Models for Isotopic Fractionation
681 Processes. Environ. Sci. Technol. 46, 2652–2660. https://doi.org/10.1021/es202587m
682 Juillot, F., Maréchal, C., Morin, G., Jouvin, D., Cacaly, S., Telouk, P., Benedetti, M.F., Ildefonse,
683 P., Sutton, S., Guyot, F., Brown, G.E., 2011. Contrasting isotopic signatures between
684 anthropogenic and geogenic Zn and evidence for post-depositional fractionation processes
685 in smelter-impacted soils from Northern France. Geochim. Cosmochim. Acta 75, 2295–
686 2308. https://doi.org/10.1016/j.gca.2011.02.004
687 Juillot, F., Maréchal, C., Ponthieu, M., Cacaly, S., Morin, G., Benedetti, M., Hazemann, J.L.,
688 Proux, O., Guyot, F., 2008. Zn isotopic fractionation caused by sorption on goethite and 2-
689 Lines ferrihydrite. Geochim. Cosmochim. Acta 72, 4886–4900.
690 https://doi.org/10.1016/j.gca.2008.07.007
691 Juillot, F., Morin, G., Ildefonse, P., Trainor, T.P., Benedetti, M., Galoisy, L., Calas, G., Brown,
692 G.E., 2003. Occurrence of Zn/Al hydrotalcite in smelter-impacted soils from northern
693 France: Evidence from EXAFS spectroscopy and chemical extractions. Am. Mineral. 88,
694 509–526. https://doi.org/10.2138/am-2003-0405
695 Kabata-Pendias, A., 2011. Trace Elements in Soils and Plants, Fourth Edition 33.
696 Kimball, B.E., Mathur, R., Dohnalkova, A.C., Wall, A.J., Runkel, R.L., Brantley, S.L., 2009.
697 Copper isotope fractionation in acid mine drainage. Geochim. Cosmochim. Acta 73, 1247–
698 1263. https://doi.org/10.1016/j.gca.2008.11.035
699 Kretzschmar, R., Schafer, T., 2005. Metal Retention and Transport on Colloidal Particles in the
700 Environment. Elements 1, 205–210. https://doi.org/10.2113/gselements.1.4.205

701 Kříbek, B., Šípková, A., Ettler, V., Mihaljevič, M., Majer, V., Knésl, I., Mapani, B., Penížek, V.,
702 Vaněk, A., Sracek, O., 2018. Variability of the copper isotopic composition in soil and
703 grass affected by mining and smelting in Tsumeb, Namibia. Chem. Geol.
704 https://doi.org/10.1016/j.chemgeo.2018.05.035
705 Lafuente, A.L., González, C., Quintana, J.R., Vázquez, A., Romero, A., 2008. Mobility of heavy
706 metals in poorly developed carbonate soils in the Mediterranean region. Geoderma 145,
707 238–244. https://doi.org/10.1016/j.geoderma.2008.03.012
708 Legros, J.P., 2007. Les grands sols du monde, Science & technologie de l'environnement. Presses
709 polytechniques et universitaires romandes.
710 Legros, S., Levard, C., Marcato-Romain, C.-E., Guiresse, M., Doelsch, E., 2017. Anaerobic
711 Digestion Alters Copper and Zinc Speciation. Environ. Sci. Technol. 51, 10326–10334.
712 https://doi.org/10.1021/acs.est.7b01662
713 Luck, J.M., Ben Othman, D., 2002a. Trace element and Pb isotope variability during rainy events
714 in the NW Mediterranean: constraints on anthropogenic and natural sources. Chem. Geol.
715 182, 443–460. https://doi.org/10.1016/S0009-2541(01)00324-2
716 Luck, J.M., Ben Othman, D., 2002b. Trace element and Pb isotope variability during rainy events
717 in the NW Mediterranean: constraints on anthropogenic and natural sources. Chem. Geol.
718 182, 443–460. https://doi.org/10.1016/S0009-2541(01)00324-2
719 Lugmair, G.., Galer, S.J.., 1992. Age and isotopic relationships among the angrites Lewis Cliff
720 86010 and Angra dos Reis. Geochim. Cosmochim. Acta 56, 1673–1694.
721 https://doi.org/10.1016/0016-7037(92)90234-A
722 Luxton, T.P., Miller, B.W., Scheckel, K.G., 2013. Zinc Speciation Studies in Soil, Sediment and
723 Environmental Samples 45.
724 Maréchal, C.N., Télouk, P., Albarède, F., 1999. Precise analysis of copper and zinc isotopic
725 compositions by plasma-source mass spectrometry. Chem. Geol. 156, 251–273.
726 https://doi.org/10.1016/S0009-2541(98)00191-0
727 Maring, H., Settle, D.M., Buat-Ménard, P., Dulac, F., Patterson, C.C., 1987. Stable lead isotope
728 tracers of air mass trajectories in the Mediterranean region. Nature 330, 154.
729 Mathur, R., Titley, S., Barra, F., Brantley, S., Wilson, M., Phillips, A., Munizaga, F., Maksaev,
730 V., Vervoort, J., Hart, G., 2009. Exploration potential of Cu isotope fractionation in
731 porphyry copper deposits. J. Geochem. Explor. 102, 1–6.
732 https://doi.org/10.1016/j.gexplo.2008.09.004
733 Mattielli, N., Petit, J.C.J., Deboudt, K., Flament, P., Perdrix, E., Taillez, A., Rimetz-Planchon, J.,
734 Weis, D., 2009. Zn isotope study of atmospheric emissions and dry depositions within a 5
735 km radius of a Pb–Zn refinery. Atmos. Environ. 43, 1265–1272.
736 https://doi.org/10.1016/j.atmosenv.2008.11.030
737 Mihaljevič, M., Jarošíková, A., Ettler, V., Vaněk, A., Penížek, V., Kříbek, B., Chrastný, V.,
738 Sracek, O., Trubač, J., Svoboda, M., Nyambe, I., 2018. Copper isotopic record in soils and
739 tree rings near a copper smelter, Copperbelt, Zambia. Sci. Total Environ. 621, 9–17.
740 https://doi.org/10.1016/j.scitotenv.2017.11.114
741 Ochoa Gonzalez, R., Weiss, D., 2015. Zinc Isotope Variability in Three Coal-Fired Power Plants:
742 A Predictive Model for Determining Isotopic Fractionation during Combustion. Environ.
743 Sci. Technol. 49, 12560–12567. https://doi.org/10.1021/acs.est.5b02402
744 Opfergelt, S., Cornélis, J.T., Houben, D., Givron, C., Burton, K.W., Mattielli, N., 2017. The
745 influence of weathering and soil organic matter on Zn isotopes in soils. Chem. Geol. 466,
746 140–148. https://doi.org/10.1016/j.chemgeo.2017.06.002

747 Phillips, D.L., Gregg, J.W., 2003. Source partitioning using stable isotopes: coping with too many
748 sources. Oecologia 136, 261–269. https://doi.org/10.1007/s00442-003-1218-3
749 Pichat, S., Douchet, C., Albarède, F., 2003. Zinc isotope variations in deep-sea carbonates from
750 the eastern equatorial Pacific over the last 175 ka. Earth Planet. Sci. Lett. 210, 167–178.
751 https://doi.org/10.1016/S0012-821X(03)00106-7
752 Pokrovsky, O.S., Viers, J., Emnova, E.E., Kompantseva, E.I., Freydier, R., 2008. Copper isotope
753 fractionation during its interaction with soil and aquatic microorganisms and metal
754 oxy(hydr)oxides: Possible structural control. Geochim. Cosmochim. Acta 72, 1742–1757.
755 https://doi.org/10.1016/j.gca.2008.01.018
756 Pokrovsky, O.S., Viers, J., Freydier, R., 2005. Zinc stable isotope fractionation during its
757 adsorption on oxides and hydroxides. J. Colloid Interface Sci. 291, 192–200.
758 https://doi.org/10.1016/j.jcis.2005.04.079
759 Ravel, B., Newville, M., 2005. ıt ATHENA, ıt ARTEMIS, ıt HEPHAESTUS: data analysis for X-
760 ray absorption spectroscopy using ıt IFEFFIT. J. Synchrotron Radiat. 12, 537–541.
761 https://doi.org/10.1107/S0909049505012719
762 Semlali, R.M., van Oort, F., Denaix, L., Loubet, M., 2001. Estimating Distributions of Endogenous
763 and Exogenous Pb in Soils by Using Pb Isotopic Ratios. Environ. Sci. Technol. 35, 4180–
764 4188. https://doi.org/10.1021/es0002621
765 Shiel, A.E., Weis, D., Orians, K.J., 2010. Evaluation of zinc, cadmium and lead isotope
766 fractionation during smelting and refining. Sci. Total Environ. 408, 2357–2368.
767 https://doi.org/10.1016/j.scitotenv.2010.02.016
768 Shotyk, W., Weiss, D., Heisterkamp, M., Cheburkin, A.K., Appleby, P.G., Adams, F.C., 2002.
769 New Peat Bog Record of Atmospheric Lead Pollution in Switzerland: Pb Concentrations,
770 Enrichment Factors, Isotopic Composition, and Organolead Species. Environ. Sci.
771 Technol. 36, 3893–3900. https://doi.org/10.1021/es010196i
772 Šillerová, H., Chrastný, V., Vítková, M., Francová, A., Jehlička, J., Gutsch, M.R., Kocourková, J.,
773 Aspholm, P.E., Nilsson, L.O., Berglen, T.F., Jensen, H.K.B., Komárek, M., 2017. Stable
774 isotope tracing of Ni and Cu pollution in North-East Norway: Potentials and drawbacks.
775 Environ. Pollut. 228, 149–157. https://doi.org/10.1016/j.envpol.2017.05.030
776 Sivry, Y., Riotte, J., Sonke, J.E., Audry, S., Schäfer, J., Viers, J., Blanc, G., Freydier, R., Dupré,
777 B., 2008. Zn isotopes as tracers of anthropogenic pollution from Zn-ore smelters The Riou
778 Mort–Lot River system. Chem. Geol. 255, 295–304.
779 https://doi.org/10.1016/j.chemgeo.2008.06.038
780 Song, S., Mathur, R., Ruiz, J., Chen, D., Allin, N., Guo, K., Kang, W., 2016. Fingerprinting two
781 metal contaminants in streams with Cu isotopes near the Dexing Mine, China. Sci. Total
782 Environ. 544, 677–685. https://doi.org/10.1016/j.scitotenv.2015.11.101
783 Sonke, J., Sivry, Y., Viers, J., Freydier, R., Dejonghe, L., Andre, L., Aggarwal, J., Fontan, F.,
784 Dupre, B., 2008. Historical variations in the isotopic composition of atmospheric zinc
785 deposition from a zinc smelter. Chem. Geol. 252, 145–157.
786 https://doi.org/10.1016/j.chemgeo.2008.02.006
787 Sossi, P.A., Halverson, G.P., Nebel, O., Eggins, S.M., 2015. Combined Separation of Cu, Fe and
788 Zn from Rock Matrices and Improved Analytical Protocols for Stable Isotope
789 Determination. Geostand. Geoanalytical Res. 39, 129–149. https://doi.org/10.1111/j.1751-
790 908X.2014.00298.x

Souto-Oliveira, C.E., Babinski, M., Araújo, D.F., Andrade, M.F., 2018. Multi-isotopic fingerprints (Pb, Zn, Cu) applied for urban aerosol source apportionment and discrimination. Sci. Total Environ. 626, 1350–1366. https://doi.org/10.1016/j.scitotenv.2018.01.192

Sterckeman, T., Douay, F., Proix, N., Fourrier, H., 2000. Vertical distribution of Cd, Pb and Zn in soils near smelters in the North of France. Environ. Pollut. 107, 377–389. https://doi.org/10.1016/S0269-7491(99)00165-7

Stos-Gale, Z., Gale, N.H., Houghton, J., Speakman, R., 1995. LEAD ISOTOPE DATA FROM THE ISOTRACE LABORATORY, OXFORD: ARCHAEOMETRY DATA BASE 1, ORES FROM THE WESTERN MEDITERRANEAN. Archaeometry 37, 407–415. https://doi.org/10.1111/j.1475-4754.1995.tb00753.x

Testiati, E., Parinet, J., Massiani, C., Laffont-Schwob, I., Rabier, J., Pfeifer, H.-R., Lenoble, V., Masotti, V., Prudent, P., 2013. Trace metal and metalloid contamination levels in soils and in two native plant species of a former industrial site: Evaluation of the phytostabilization potential. J. Hazard. Mater. 248–249, 131–141. https://doi.org/10.1016/j.jhazmat.2012.12.039

Thapalia, A., Borrok, D.M., Van Metre, P.C., Musgrove, M., Landa, E.R., 2010. Zn and Cu Isotopes as Tracers of Anthropogenic Contamination in a Sediment Core from an Urban Lake. Environ. Sci. Technol. 44, 1544–1550. https://doi.org/10.1021/es902933y

Véron, A., Flament, P., Bertho, M.L., Alleman, L., Flegal, R., Hamelin, B., 1999. Isotopic evidence of pollutant lead sources in Northwestern France. Atmos. Environ. 33, 3377–3388. https://doi.org/10.1016/S1352-2310(98)00376-8

Viers, J., Grande, J.A., Zouiten, C., Freydier, R., Masbou, J., Valente, T., Torre, M.-L. de la, Destrigneville, C., Pokrovsky, O.S., 2018. Are Cu isotopes a useful tool to trace metal sources and processes in acid mine drainage (AMD) context? Chemosphere 193, 1071–1079. https://doi.org/10.1016/j.chemosphere.2017.11.133

Viers, J., Oliva, P., Nonell, A., Gélabert, A., Sonke, J.E., Freydier, R., Gainville, R., Dupré, B., 2007. Evidence of Zn isotopic fractionation in a soil–plant system of a pristine tropical watershed (Nsimi, Cameroon). Chem. Geol. 239, 124–137. https://doi.org/10.1016/j.chemgeo.2007.01.005

Voegelin, A., Jacquat, O., Pfister, S., Barmettler, K., Scheinost, A.C., Kretzschmar, R., 2011. Time-Dependent Changes of Zinc Speciation in Four Soils Contaminated with Zincite or Sphalerite. Environ. Sci. Technol. 45, 255–261. https://doi.org/10.1021/es101189d

Voegelin, A., Pfister, S., Scheinost, A.C., Marcus, M.A., Kretzschmar, R., 2005. Changes in zinc speciation in field soil after contamination with zinc oxide. Env. Sci Technol 39, 6616.

von Storch, H., Costa-Cabral, M., Hagner, C., Feser, F., Pacyna, J., Pacyna, E., Kolb, S., 2003. Four decades of gasoline lead emissions and control policies in Europe: a retrospective assessment. Sci. Total Environ. 311, 151–176. https://doi.org/10.1016/S0048-9697(03)00051-2

Weinstein, C., Moynier, F., Wang, K., Paniello, R., Foriel, J., Catalano, J., Pichat, S., 2011. Isotopic fractionation of Cu in plants. Chem. Geol. https://doi.org/10.1016/j.chemgeo.2011.05.010

Weiss, D., Shotyk, W., Boyle, E.A., Kramers, J.D., Appleby, P.G., Cheburkin, A.K., 2002. Comparative study of the temporal evolution of atmospheric lead deposition in Scotland and eastern Canada using blanket peat bogs. Sci. Total Environ. 292, 7–18. https://doi.org/10.1016/S0048-9697(02)00025-6

836 Weiss, D.J., Rehkdmper, M., Schoenberg, R., McLaughlin, M., Kirby, J., Campbell, P.G.C.,
837 Arnold, T., Chapman, J., Peel, K., Gioia, and S., 2008. Application of Nontraditional
838 Stable-Isotope Systems to the Study of Sources and Fate of Metals in the Environment.
839 Environ. Sci. Technol. 42, 655–664. https://doi.org/10.1021/es0870855
840 Wen, H., Zhang, Y., Cloquet, C., Zhu, C., Fan, H., Luo, C., 2015. Tracing sources of pollution in
841 soils from the Jinding Pb–Zn mining district in China using cadmium and lead isotopes.
842 Appl. Geochem. 52, 147–154. https://doi.org/10.1016/j.apgeochem.2014.11.025
843 Wiederhold, J.G., 2015. Metal Stable Isotope Signatures as Tracers in Environmental
844 Geochemistry. Environ. Sci. Technol. 49, 2606–2624. https://doi.org/10.1021/es504683e
845 Wilkinson, J.J., Weiss, D.J., Mason, T.F.D., Coles, B.J., 2005. Zinc isotope variation in
846 hydrothermal systems: preliminary evidence from the Irish Midlands ore field 8.
847 World Health Organization, Food and Agriculture Organization of the United Nations,
848 International Atomic Energy Agency (Eds.), 1996. Trace elements in human nutrition and
849 health. World Health Organization, Geneva.
850 Yanful, E.K., Quigley, R.M., Wayne Nesbitt, H., 1988. Heavy metal migration at a landfill site,
851 Sarnia, Ontario, Canada—2: metal partitioning and geotechnical implications. Appl.
852 Geochem. 3, 623–629. https://doi.org/10.1016/0883-2927(88)90094-7
853 Yin, N.-H., Sivry, Y., Benedetti, M.F., Lens, P.N.L., van Hullebusch, E.D., 2016. Application of
854 Zn isotopes in environmental impact assessment of Zn–Pb metallurgical industries: A mini
855 review. Appl. Geochem. 64, 128–135. https://doi.org/10.1016/j.apgeochem.2015.09.016
856

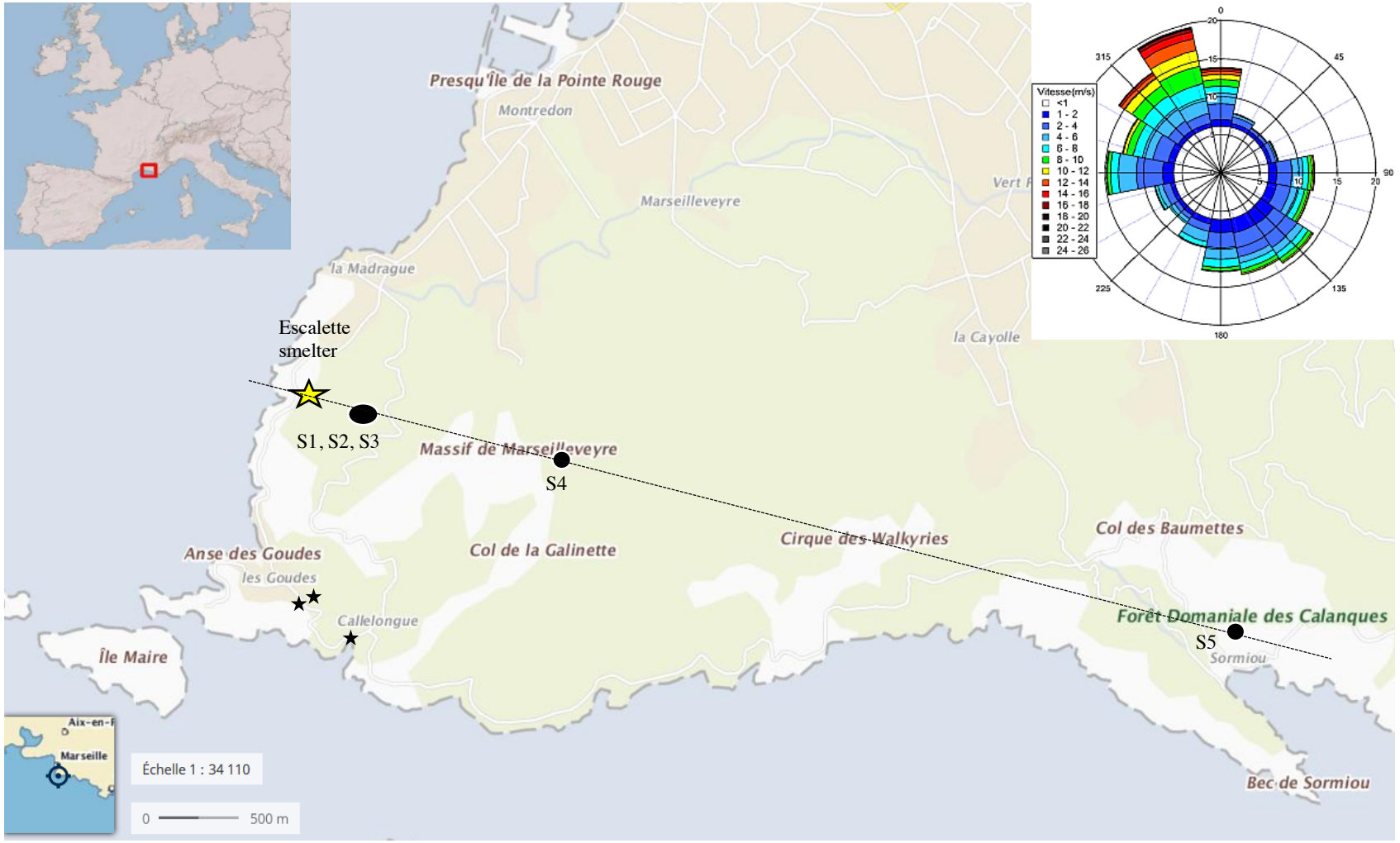
Presqu'île de la Pointe Rouge
Montredon
Marseilleveyre
la Madrague
la Cayolle
Escalette
smelter
S1, S2, S3
Massif de Marseilleveyre
S4
Anse des Goudes
les Goudes
Col de la Galinette
Cirque des Walkyries
Col des Baumettes
Callelongue
Île Maire
Forêt Domaniale des Calanques
S5
Sormiou
Bec de Sormiou
Marseille
Échelle 1 : 34 110
0
500 m
Vitesse(m/s)
<1
1 - 2
2 - 4
4 - 6
6 - 8
8 - 10
10 - 12
12 - 14
14 - 16
16 - 18
18 - 20
20 - 22
22 - 24
24 - 26

Figure 1

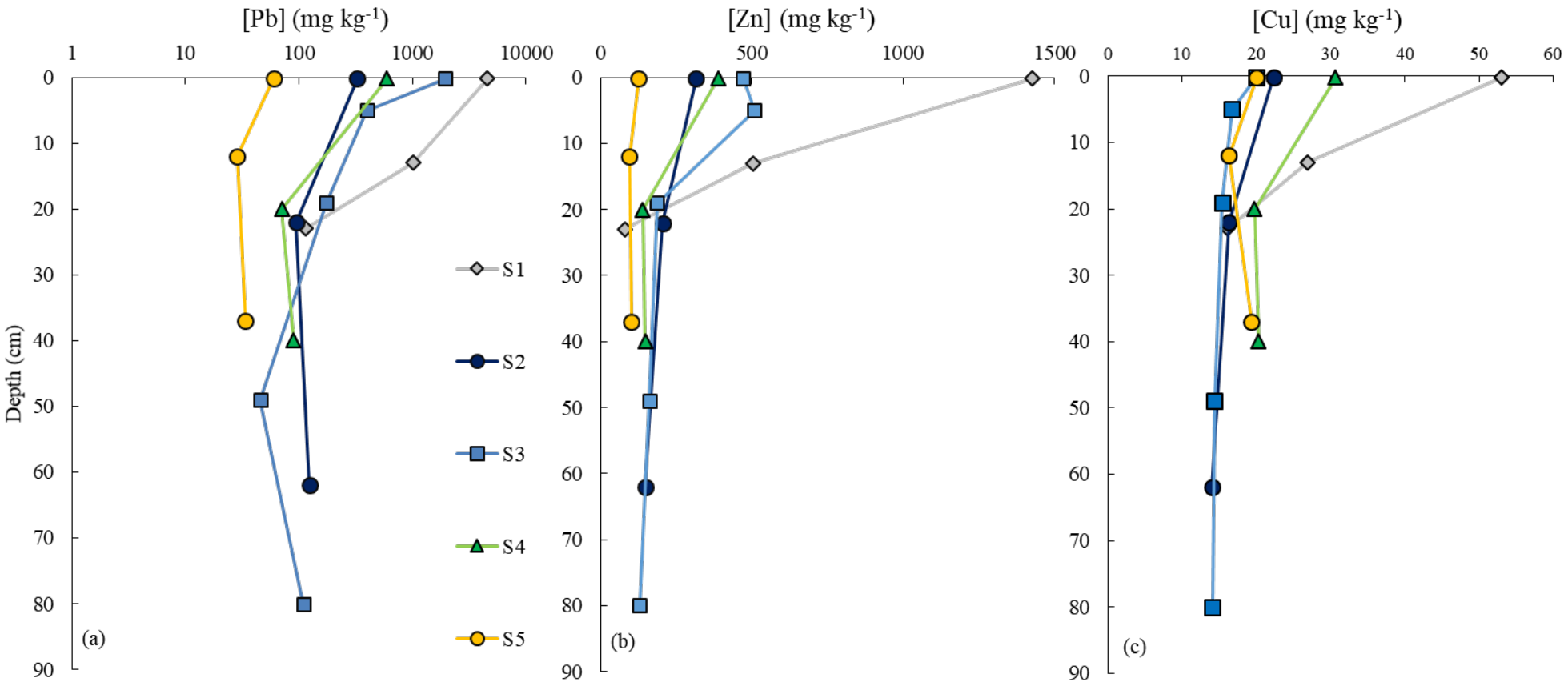
[Pb] (mg kg-1)
1
10
100
1000
10000
[Zn] (mg kg-1)
0
500
1000
1500
[Cu] (mg kg-1)
0
10
20
30
40
50
60
Depth (cm)
0
10
20
30
40
50
60
70
80
90
S1
S2
S3
S4
S5
(a)
(b)
(c)

Figure 2

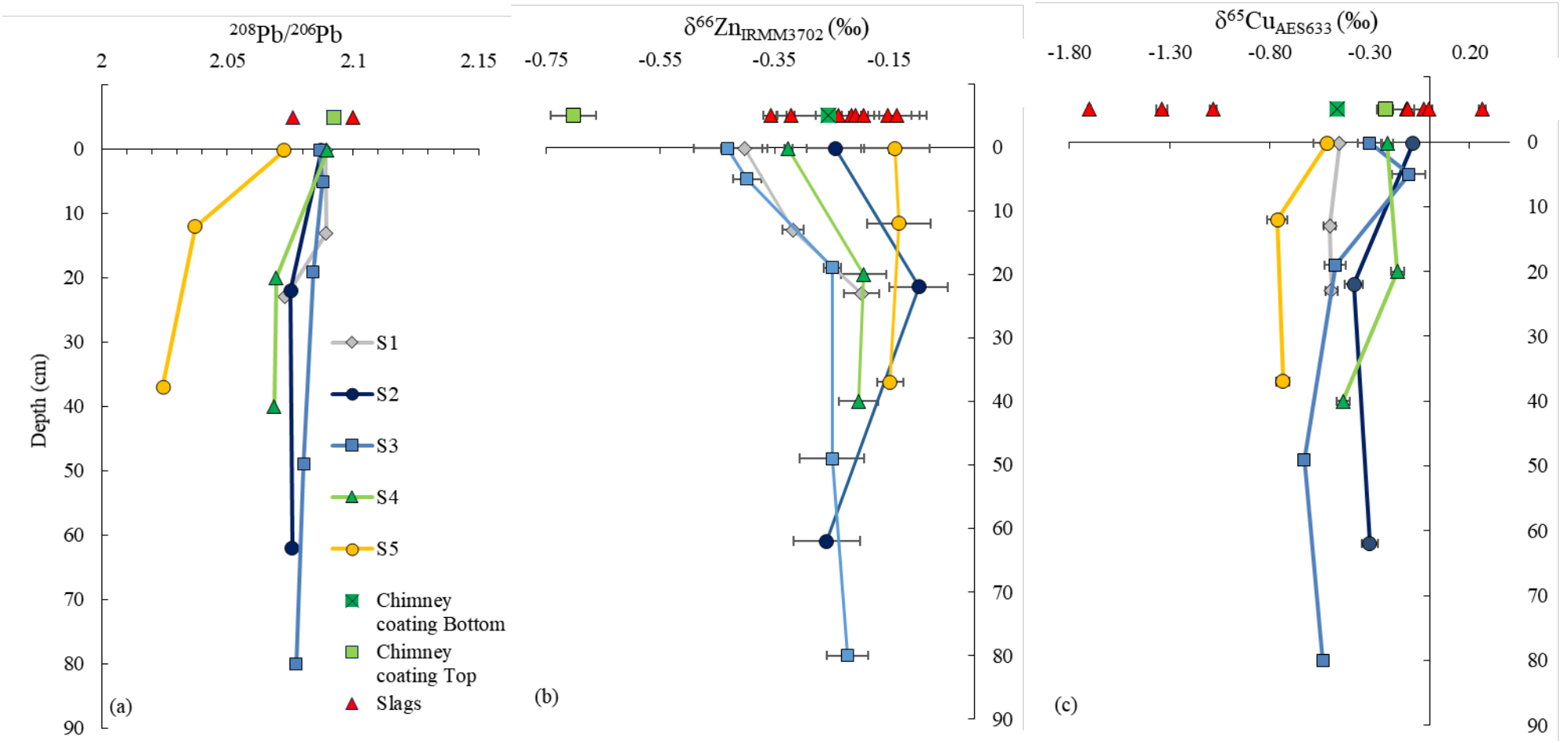
$^{208}Pb/^{206}Pb$
2
2.05
2.1
2.15
$\delta^{66}Zn_{IRMM3702}$ (‰)
-0.75
-0.55
-0.35
-0.15
$\delta^{65}Cu_{AES633}$ (‰)
-1.80
-1.30
-0.80
-0.30
0.20
Depth (cm)
0
10
20
30
40
50
60
70
80
90
S1
S2
S3
S4
S5
Chimney coating Bottom
Chimney coating Top
Slags
(a)
(b)
(c)

Figure 3

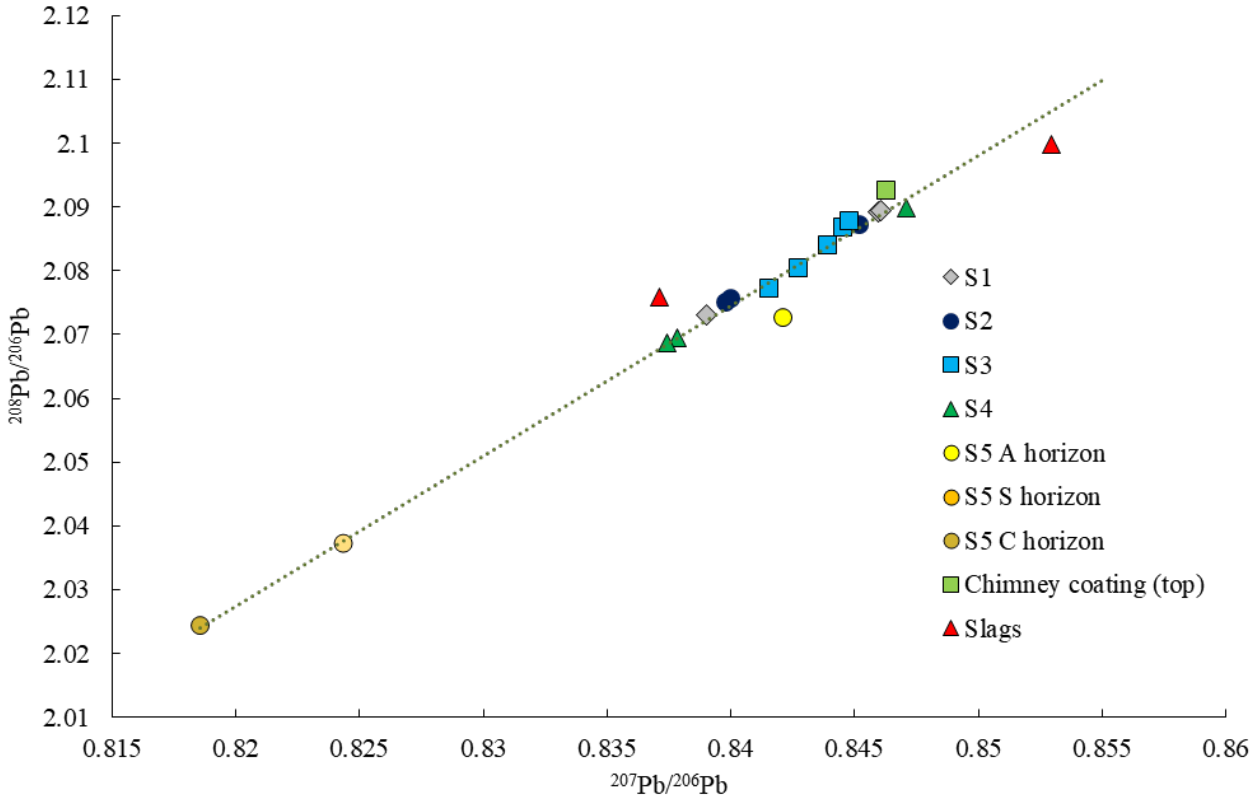
2.12
2.11
2.1
2.09
2.08
2.07
2.06
2.05
2.04
2.03
2.02
2.01
208Pb/206Pb
0.815
0.82
0.825
0.83
0.835
0.84
0.845
0.85
0.855
0.86
207Pb/206Pb
S1
S2
S3
S4
S5 A horizon
S5 S horizon
S5 C horizon
Chimney coating (top)
Slags

Figure 4a

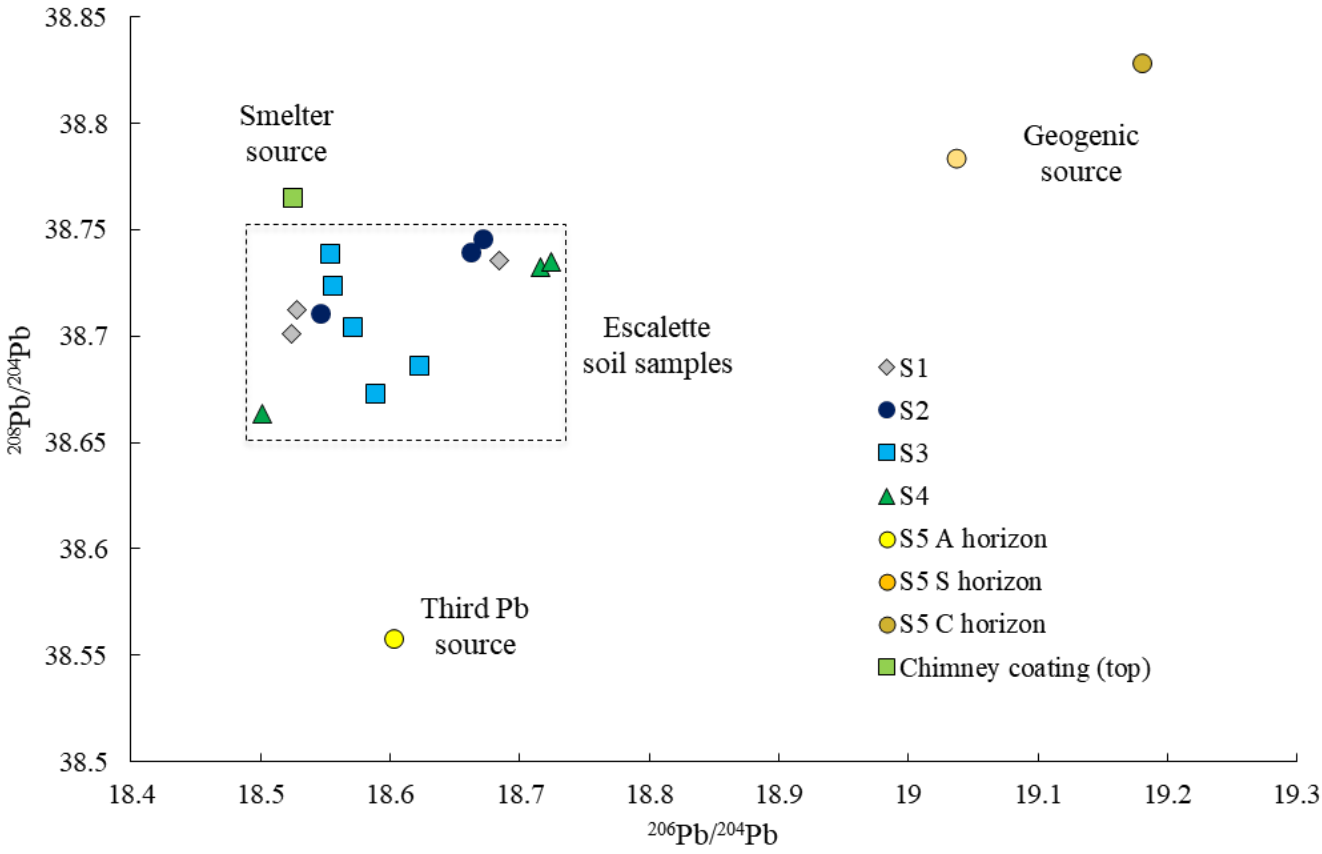
38.85
38.8
38.75
38.7
38.65
38.6
38.55
38.5
208Pb/204Pb
18.4
18.5
18.6
18.7
18.8
18.9
19
19.1
19.2
19.3
206Pb/204Pb
Smelter source
Geogenic source
Escalette soil samples
Third Pb source
S1
S2
S3
S4
S5 A horizon
S5 S horizon
S5 C horizon
Chimney coating (top)

Figure 4b

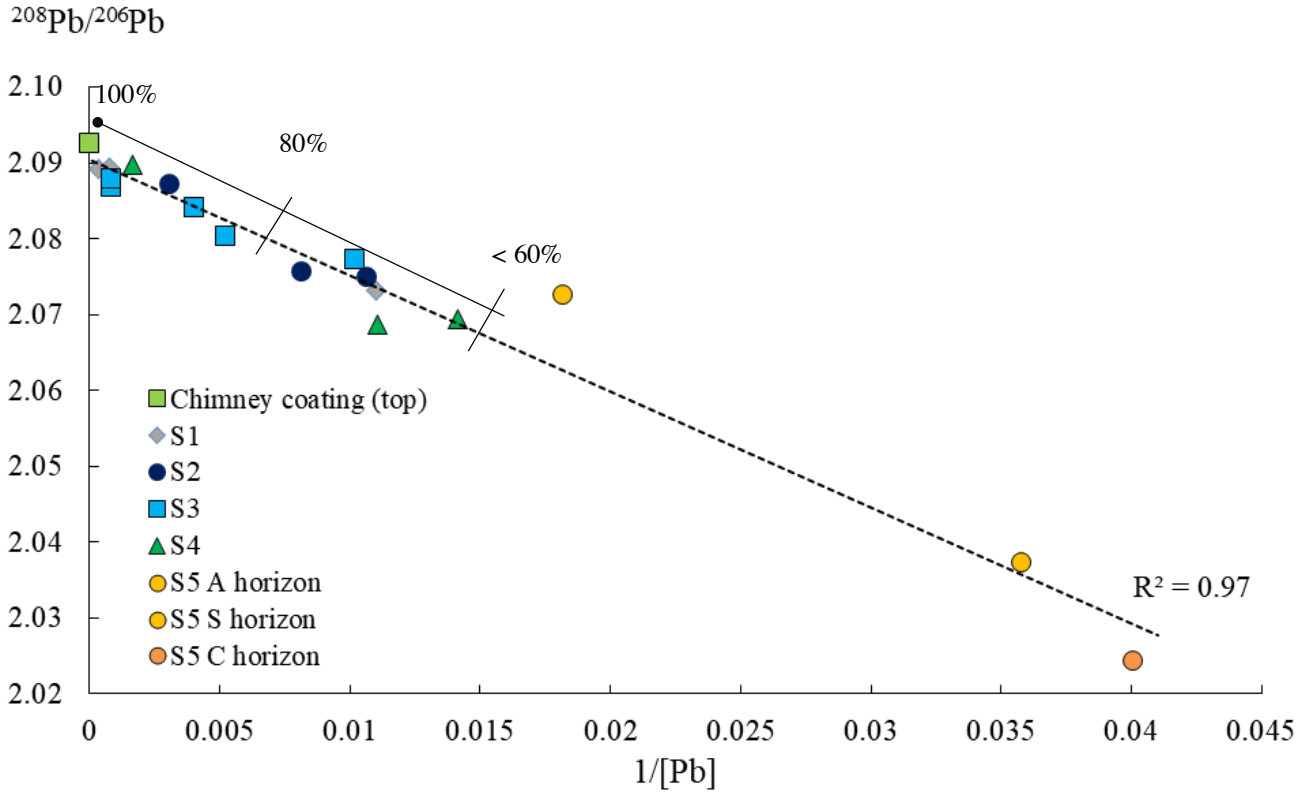
208Pb/206Pb
2.10
2.09
2.08
2.07
2.06
2.05
2.04
2.03
2.02
100%
80%
< 60%
Chimney coating (top)
S1
S2
S3
S4
S5 A horizon
S5 S horizon
S5 C horizon
R² = 0.97
0
0.005
0.01
0.015
0.02
0.025
0.03
0.035
0.04
0.045
1/[Pb]

Figure 5

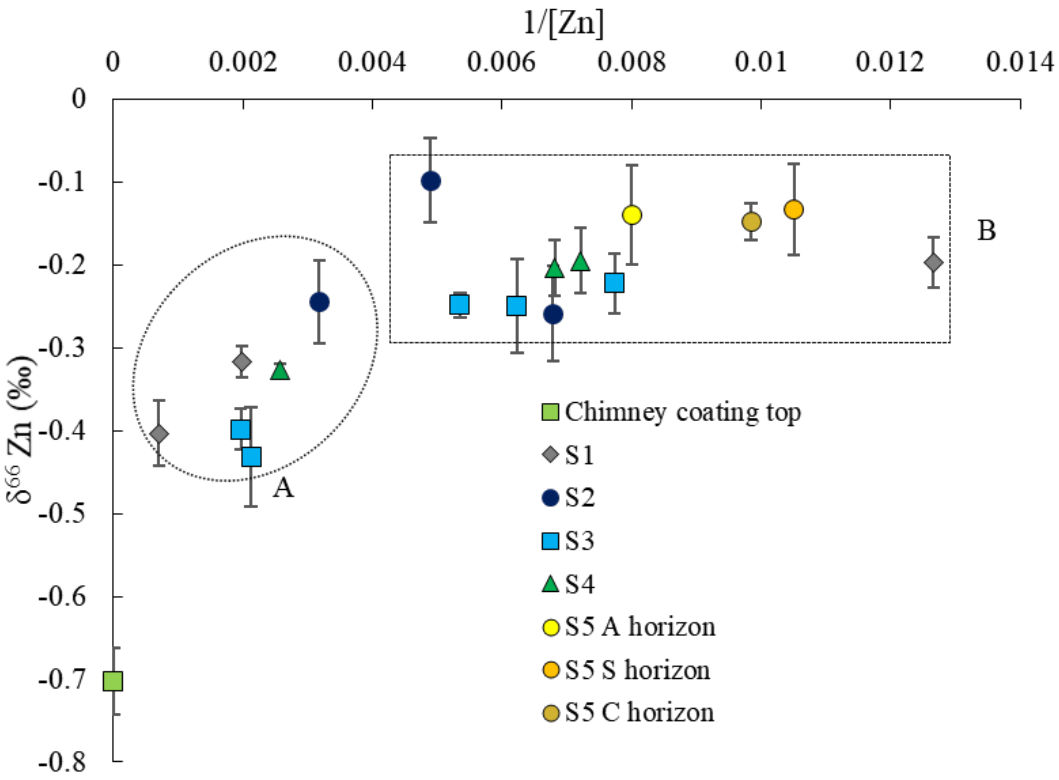
1/[Zn]
0
0.002
0.004
0.006
0.008
0.01
0.012
0.014
0
-0.1
-0.2
-0.3
-0.4
-0.5
-0.6
-0.7
-0.8
δ66 Zn (‰)
A
B
Chimney coating top
S1
S2
S3
S4
S5 A horizon
S5 S horizon
S5 C horizon

Figure 6

Figure Captions

Figure 1: Global Marseilleveyre Massif map near Marseilles (France). Average wind directions over 10 years (2001-2011) obtained from Marignane station (MétéoFrance, 2011). Dotted line indicates the 7 km NW-SE studied transect with relative position of the soil profiles under the main wind NNW from the Escalette smelter (yellow star) to S5 soil (black dot). Black stars highlight the position of other industries (Pb smelter (1854-1878), soda-production factory (1854-1894), sulfur refinery (1860-1900) operating at the beginning of the Escalette smelter exploitation (1851-1925).

Figure 2: Concentration (mg kg^{-1}) profiles of Pb (a), Zn (b) and Cu (c) in sampled soils. For Pb concentrations (a) note the logarithmic scale.

Figure 3: Evolution of Pb (a), Zn (b) and Cu (c) isotopic signatures of soils with depth. For clarity, results obtained on the smelter samples (slags and chimney) are placed above the surface level. Error bars represent the two standard deviations (2SD) calculated from three analyses of the same sample. Calculated 2SD for Pb ratios are $<10^{-4}$ and are printed in smaller type than the symbols. In the $^{208}Pb/^{206}Pb$ plot (a), the two chimney coatings (top and bottom) overlap due to their identical Pb isotopic compositions. Soil sample symbols are placed at the top of their respective horizons. Only two slags (1,2) were analyzed for their Pb isotopic signatures while 7 slags were analyzed for Zn and Cu.

Figure 4a: Mixing trend of all sampled soils and smelter samples in a $^{208}Pb/^{206}Pb$ vs $^{207}Pb/^{206}Pb$ plot. Calculated 2SD for Pb ratios are $<10^{-4}$ and are printed in smaller type than the symbols. End members are represented by (i) the uncontaminated deepest horizon of the S5 profile (S5 C) and (ii) the chimney coatings. The dotted line represents the linear trend (r^2 = 0.98, p value=$1.47E^{-16}$). For a given soil profile (except for S5), all horizons are represented by identical symbols. For S5, individual horizons are distinguished using the same symbols but different

colors. Only slags 1 and 2 were analyzed for Pb isotopic compositions and are presented here (see Table S1c).

Figure 4b: Plot of $^{208}Pb/^{204}Pb$ vs $^{206}Pb/^{204}Pb$. Lead isotopes of the Escalette soil samples (highlighted by the dotted black square) are constrained in a three Pb source domain: smelter source (i.e. the chimney coating top), geogenic source (i.e. S5 deepest horizon) and a third source (i.e. atmospheric aerosol) only visible on the S5 A horizon. Calculated 2SD for Pb ratios are $<10^{-4}$ and printed smaller than the symbols.

Figure 5: Plot of $^{208}Pb/^{206}Pb$ vs 1/[Pb] total concentrations. A two end-member mixing line (dotted line, $r^2=0.97$; p value=$2.84E^{-13}$) connects the chimney sample (top) and the deepest horizon of the S5 profile (C). Soils from S1 to S4 plotted along the mixing line, indicating that their total Pb concentrations represent a mixture of anthropogenic Pb from the smelter ($^{208}Pb/^{206}Pb$: 2.0922), and natural Pb, from the geogenic background ($^{208}Pb/^{206}Pb$: 2.0243). The contribution of anthropogenic Pb to the total Pb (%), presented in Table S, is reported as a solid black line, close to the mixing line.

Figure 6: Plot of $\delta^{66}Zn$ values (‰) vs 1/[Zn]. Zinc isotopic signatures of the soils cannot be explained by binary mixing. Two distinct Zn pools, labeled A and B, and highlighted by a circle and rectangle in dashed lines can be distinguished. Error bars represent the 2SD associated to $\delta^{66}Zn$ values. A: pool dominated by anthropogenic Zn from the smelter, observed in S1, S2, S3 and S4 surface horizons. Discrepancy between $\delta^{66}Zn$ values of the soils and the chimney sample can be explained by isotopic fractionation during precipitation of Zn-Layered-Double-Hydroxide in the surface horizons. B: pool dominated by natural Zn observed in all other subsurface horizons and in the S5 soil profile and originating from the natural geogenic background modified by pedogenetic processes.